Catalytic activities of titania-supported nickel for carbon-dioxide methanation

Preeya Unwiset[a], Kingkaew Chayakul Chanapattharapol[a]*,

Pinit Kidkhunthod[b], Yingyot Poo-arporn[b], Bunsho Ohtani[c]

[a]*Materials Chemistry Research Center, Department of Chemistry and Center of Excellence for Innovation in Chemistry, Faculty of science, Khon Kaen University, Khon Kaen, 40002, Thailand*

[b]*Synchrotron Light Research Institute, 111 University Avenue, Muang District, Nakhon Ratchasima, 30000, Thailand*

[c]*Institute for Catalysis, Hokkaido University, Sapporo 001-0021, Japan*

*Corresponding author. Tel: +66 430 09700 ext. 12371, Fax: +66 432 02373.

E-mail address: kingkaew@kku.ac.th (K.C. Chanapattharapol).

Abstract

Titania (TiO_2)-supported nickel (Ni) catalysts (3, 6, 12 and 20wt%; Ni/TiO_2) were prepared by a sol-gel method to be used as a catalyst for carbon-dioxide (CO_2) methanation. The catalytic activity tests were conducted with a fixed-bed reactor in the temperature range of 100–550 °C. The results showed that the CO_2 conversion increased with increasing Ni content and 20wt% Ni/TiO_2 exhibited the highest CO_2 conversion and the methane (CH_4) yield which corresponded to the lowest apparent activation energy. Moreover, 20wt% Ni/TiO_2 also showed high stability under the CO_2 methanation stream for 72 h. The addition of Ni into TiO_2 during the sol-gel process modified the catalyst properties which affected to their catalytic activities, and the influence of Ni addition on the catalyst structure was studied by several techniques. The results on XRD and EXAFS revealed unit cell expansion and lattice distortion which indicated that nickel(II) cation was incorporated into TiO_2 lattice. Upon increasing in Ni content, the nickel(II) oxide (NiO) phase was observed indicating the high crystallinity of NiO and suppression of TiO_2 crystal growth. These effects led to smaller crystalline size of TiO_2 and higher surface area of the catalysts. The oxidation states of nickel and titanium were analyzed to be +2 and +4, respectively for fresh catalysts. After pretreatment by hydrogen (H_2), Ni(II) was converted to Ni(0) and this electronic state was still unchanged during the course of methanation while Ti(IV) was kept unaltered for fresh catalysts and those during the reaction. However, the distortion or defect around Ti(IV) ions in Ni-loaded TiO_2 was observed as increase in Ti K-edge XANES pre-edge peaks. The addition of Ni led to formation of oxygen vacancy in TiO_2 lattice and NiO-phase formation which might act as the sites for CO_2

and H_2 adsorption, respectively. Therefore, higher amount of adsorbed CO_2 and H_2 could enhance the surface reaction and also speed up the CO_2-methanation.

Keywords: carbon-dioxide methanation; titania-supported nickel; XANES; EXAFS

1. Introduction

Recently, global warming is the most concerned problem of the world. The main reason for this problem is releasing high level of greenhouse gases (GHG) into the atmosphere. Carbon dioxide (CO_2) has a large proportion of GHG. Enormous CO_2 emission level is a mainly result from human activities such as burning fossil fuel (coal, natural gas, and oil), transportation, deforestation, agriculture, electricity and industrial sectors. Therefore, reduction and utillization of CO_2 to produce value-added raw meterials for chemical reactions are intersted. CO_2 methanation is one of a powerful approach to utillize the CO_2 as a feedstock for producing CH_4. This reaction is called the Sabatier reaction which is defied as the following equation;

$$CO_2 + 4H_2 \rightleftharpoons CH_4 + 2H_2O \qquad \Delta H_{298K} = -165 \text{ kJ mol}^{-1} \qquad (1)$$

The characteristic of this reaction are as follows; i) this reaction is a highly exothermic process, thus, CH_4 formation prefers to occur at low temperature and high pressure [1,2] ii) there is a kinetic barrier with eight-electron reduction process of the CO_2 (4+) to form CH_4 (4-) iii) CO_2 molecule is a strong linear structure with two double bond, so high dissociation energy must be consumed and iv) side reaction, reverse water gas shift ($CO_2 + 4H_2 \rightleftharpoons CO + 2H_2O$) [3], occurs usually at high temperature which can produce an undesired product (CO). Therefore, from these limitations of this reaction, to increase the rate at low temperature, the catalyst must be employed.

Normally, the catalyst is consisted of two components; support and active component. The typical support properties are chemical stability, high thermal resistance and high surface area and porosity. The last properties have a significant role in catalytic reaction, since the adsorption and surface reaction processes are occurred on catalyst surface. An active component is another important component which is usually added onto the support with a small amount when compared with support. The function of an active site is selectively toward on adsorption of reactants, thus, an appropriate selectively active component is used for enhancing the adsorption and also speed-up the surface reaction. Consequently, tuning and modifying these two components properties can control and dominate the catalytic performance of the catalyst. For CO_2 methanation, enhancing the adsorption ability of two

reactants (CO_2 and H_2) on catalyst surface can possibly improve the surface reaction between these two absorbed species and then the product formation rate also increases. Therefore, modifying catalyst with appropriate active site for CO_2 and H_2 adsorption can enhance the reaction rate. It is well known that H_2 favors to adsorb on metal, especially transition metal group, various active metals are widely used for this reaction such as Rh, Ru, Pt and Pd [4-7]. However, using the noble metals are limited due to their high cost and scarcity [8]. From this reason, nickel is more attractive to be used for CO_2 methanation due to its relatively low price and also give high activity [9-11]. In order to enhance the H_2 adsorption capacity, high dispersion of active metal on catalyst surface must be done. However, Ni can be deactivated by using at high temperature due to sintering process, thus, modifying the catalyst with resistance of this effect is also of interested. For CO_2 adsorption, providing the basic sites on catalyst surface can improve the CO_2 uptake via acid-base interaction. For this aspect, addition of basic metal oxide such as La_2O_3, CeO_2 and MgO is usually employed. Other method to increase CO_2 uptake is to produce an oxygen vacancy which is reported as an adsorption site for CO_2 molecule [12,13]. Oxygen vacancy can be formed within the metal oxide support by substitution of the host metal by adding metal with lower oxidation state than that of host metal [14,15]. Formation of oxygen vacancy by this way is usually used with a reducible support (TiO_2, CeO_2, ZrO_2, etc.), since the oxygen vacancy can mobile inside the lattice and plays an important role in redox process. Finally, it is seen that tuning and modifying of catalyst properties by considering the characteristic of reaction can produce the catalyst with great catalytic performance. It is reported that the synthesis method is strongly determined the physical and chemical properties of catalyst [11,16]. Many synthesis methods were reported to be used and provided a great catalytic performance [6,17,18]. However, the simple, environment friendly and inexpensive processes were usually preferred. The sol-gel method is one of the simplest and the most widely used due to its low cost of the required instrument, mild synthesis condition and also providing high homogeneous of the catalyst.

In this work, Ni was selected to be used as an active metal and TiO_2 was a support. Since using TiO_2 as a catalyst support for CO_2 methanation is still developed, thus it is challenging to modify TiO_2 catalysts which provide the excellent activity and produce the desired products for this reaction. Sol-gel method was used as a synthesis method to produce Ni/TiO_2 catalysts with different Ni loading. The structural and surface properties of synthesized samples upon addition of Ni was investigated by X-ray diffraction (XRD), N_2 adsorption-desorption, transmission electron microscopy (TEM), H_2 temperature-programmed reduction (TPR), H_2 chemisorption and thermogravimetric analysis. All strategies were used for studying

the effect of Ni addition for CO_2 methanation. Advanced analysis of local structures and oxidation sates of probe metals (Ni and Ti) was determined by using X-ray absorption spectroscopy (XAS) which was including with X-ray absorption near-edge structure (XANES) and extended X-ray-absorption fine structure (EXAFS). The effect of Ni addition to enhance the CO_2 methanation was discussed based on the all characterized results.

2. Experimental

2.1 Syntheses of TiO_2 and Ni-loaded TiO_2 catalysts

All synthesized samples were prepared by sol-gel method using titanium(IV) isopropoxide (98%, Acros Organics) as a precursor. For pure TiO_2, Ti precursor was mixed with glacial acetic acid (RCI Labscan) and 2-propanol (Carlo Erba Reagents*)* and then stirred for 30 min. The mixture was dropped wise with deionized water (DI) and vigorously stirred for starting hydrolysis reaction. Finally, the solution was dried in an oven at 110°C for 24 h and calcined at 500°C for 2 h to obtain bare TiO_2.

In preparation of Nickle (Ni) modified TiO_2 catalysts, the titanium(IV) isopropoxide, glacial acetic acid and 2-propanol were mixed with the same manners as the above-mentioned pure-TiO_2 preparation. The desired amount of nickel nitrate (Carlo Erba Reagents*)* was dissolved with DI water and then dropped wise in the Ti precursor mixture. The solution was dried and calcined at the same conditions as pure TiO_2. The synthesized samples were denoted as *X*wt% Ni/TiO_2 where X = 3, 6, 12 and 20wt%.

2.2 Characterization

The structural properties of synthesized samples were characterized by X-ray diffraction (XRD) using Rigaku SmartLab X-ray diffractometer using Cu K_α (λ = 0.154 nm). The XRD pattern was collected in the 2θ range of 10° to 80°. Bragg's equation was used to determine the unit cell parameters of samples by using (101) crystallographic plane of anatase TiO_2. The means of crystallite sizes of TiO_2 and Ni-loaded TiO_2 were calculated by the Scherer's equation:

$$D = \frac{K\lambda}{\beta \cos\theta} \quad (2)$$

where D is the crystallite size, K is the shape factor, λ is the X-ray wavelength, β is the broadening at half maximum and θ is the diffraction angle. In order to determine the strain induced by addition of Ni, the Williamson-Hall (W-H) plot method was used which can be expressed by the following equation;

$$\beta \cos\theta = \frac{K\lambda}{D} + 4\varepsilon \sin\theta \quad (3)$$

where ε is the strain induced from crystal imperfection and distortion. The W-H plot shows a relationship between $\beta \cos\theta$ and $4\sin\theta$. The strain (ε) can be estimated from the slope of linear fit and the crystallite size (D) can also be determined from y-intercept.

Nitrogen (N_2) adsorption-desorption isotherms were recorded using a Quantachrome (previously Yuasa Ionics; Autosorb 6AG) surface-area and pore-size analyzer. Prior N_2 adsorption, the sample was degassed at 200 °C for 2 h to remove the moisture on surface sample. Specific surface area, average pore size and pore volume were calculated by Brunnauer-Emmett-Teller (BET) equation. The specific surface area was commonly determined at relative pressure (P/P_0) range between 0.1 to 0.3. Barrett-Joyner-Halenda (BJH) method was used to calculate the pore size distribution. The pore volume was measured at the relative pressure closed to unity ($P/P_0 \sim 1$).

Hydrogen (H_2) temperature-programmed reduction (TPR) was investigated by a Belcat B apparatus. A 20-mg portion of sample was pretreated by flowing with helium (He) at 120 °C for 30 min to clean up the surface. After cooling down, the mixture gases of H_2 and argon (Ar) were flowed over the sample while the temperature was rose up to 1000 °C with ramping rate of 10 K min^{-1}. Thermal conductivity detector (TCD) was used to collect the change of thermal conductivity of the gas stream. H_2 consumption was plotted as a function of temperature.

Transmission electron microscopy were performed by TEM, a FEI Tecnai G2 20 S-TWIN), to analyze particles sizes and morphologies of samples. The catalyst particles were dispersed in ethanol by sonication before dropping on copper grids.

Inductively coupled plasma-optical emission spectroscopy (ICP-OES) analysis was employed to measure the Ni contents. The powder (0.025 g) of sample was digested by a mixture of concentrated H_2SO_4 (6 mL) and 30% H_2O_2 (2 mL). The calibration curve was in the range of 0-30 ppm. An Optima 100 DVICO-OES (PerkinElmer) instrument was used to analyze Ni contents in a sample solution. The plasma was generated by an RF power with 1300W, and plasma flow rate was 15 L/min. Auxillary and neubilizer flow rate was 0.2 L/min and 0.8 L/min, respectively. Emission light signal was detected by a CCD-array detector.

2.3 H_2 chemisorption and CO_2 uptake

H_2 chemisorption experiment was used to investigate the metal active sites on the catalyst surface which play an important role in enhancing the reaction rate. The H_2

chemisorbed amount of all-loaded samples (3, 6, 12 and 20wt% Ni/TiO_2) was carried out by Quantachrome Autosorb-1-C instrument. 200 mg of catalyst was first pretreated by flowing with He at 120 °C (ramp rate 20 °C min^{-1}) for 30 min. After pretreatment, H_2 (99.999%, Thai Industrial Gas) was flowed over the sample during rising the temperature up to 300 °C (ramp rate 20 °C min^{-1}) and the temperature was kept constant at this point for 120 min. Next, the sample was cooled down to 40 °C under vacuum and then H_2 was sequentially added to the sample. The amount of H_2 chemisorption was obtained by extrapolating method of the graph between volume of H_2 uptake and pressure. The monolayer of H_2 uptake (N_m; μmol g^{-1}) can be calculated by the following equation;

$$N_m = 44.61\ V_m \quad (4)$$

where V_m is the volume of monolayer uptake which can be determined by extrapolating method. CO_2 adsorption capacity of sample can be also used to explain the role of catalyst to catalyze the reaction rate. The CO_2 uptake was monitored by thermalgravimetric analysis (TGA, Pyris Diamond, Perkin Elmer Instrument). Al_2O_3 was used as a reference. First, the synthesized sample was separately weighted and put on the aluminum pan and then placed on the sample holder. The maximum different weight between sample and reference was 0.5 mg. The sample was first pretreated by heating at 150 °C (10 °C min^{-1}) for 45 min under N_2 flowing to remove an impurities. After that, CO_2 uptake was started by cooling down the sample to 40 °C under CO_2 flowing (100 mL min^{-1}) for 60 min. Upon decreasing the temperature, the weight of sample was increased due to adsorption of CO_2 on solid surface. The CO_2 uptake can be calculated by differentiate the weight before and after adsorption.

2.4 CO_2 methanation catalytic activity test

The CO_2 methanation-activity test was carried out in a fixed bed reactor with inner diameter of 0.6 mm. 50 mg of sample was placed at middle of pyrex reactor tube and sandwiched with quartz wool. Accurate temperature was monitored by K-type thermocouple which was located on the top of catalyst bed. The flow rates of the reactant gases were precisely controlled by mass flow controllers. Prior activity test, the synthesized catalyst was reduced under H_2 flow (50 mL min^{-1}) at 450°C and maintained for 90 min. After that, the system was cooled down to 150°C to start the reaction. H_2 and CO_2 was used as a feed gas with a ratio of H_2/CO_2 = 4 (balance with He). Total flow rate of feed gas was 40 mL min^{-1} and GHSV was 48,000 mL g^{-1} min^{-1}. The reaction temperatures were in the range of 100-550 °C. The effluent products and remaining reactants were analyzed by an online gas chromatography (Agilent

198 6890N Series, Agilent Technology) equipped with HEYSEP D Packed Column and TCD
199 detector. Instrumental diagram of CO_2 methanation catalytic activity test set up is shown in
200 Figure 1. CO_2 conversion, CH_4 and CO selectivity and yield were calculated by the following
201 equations:

202 $$X_{CO_2} = \left(\frac{F_{CO_{2in}} - F_{CO_{2out}}}{F_{CO_{2in}}} \right) \times 100 \quad (5)$$

203 $$S_{CH_4,\,CO} = \left(\frac{F_{CH_{4out}},\ _{CO_{out}}}{F_{CH_{4out}} + F_{CO_{out}}} \right) \times 100 \quad (6)$$

204 $$Y_{CH_4,\,CO} = \left(\frac{X_{CO_2} \times S_{CH_4,\,CO}}{100} \right) \quad (7)$$

205 where, X_{CO_2} is the CO_2 conversion, S is the selectivity and Y is the yield. F is the molar flow
206 rate of gas (mol s^{-1}).

207 The rate of CO_2 methanation were measured in the temperature range of 240-290 °C
208 to keep below 10% of CO_2 conversion. The rate of reaction was calculated using the following
209 equation [19];

210 $$\text{Rate} = \left(\frac{F_{CO_2}}{W} \right) \times X_{CO_2} \quad (8)$$

211 where, F_{CO_2} is the flow rate of CO_2 (mol s^{-1}), W represents the weight of catalyst (g).

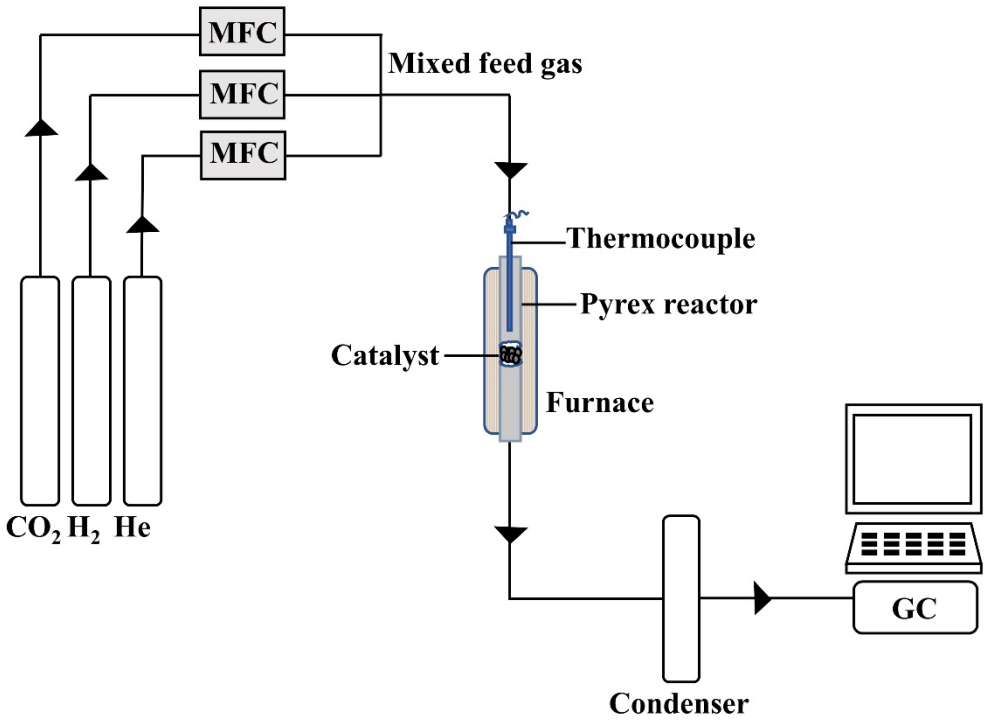

Figure 1 Instrumental diagram of CO_2 methanation catalytic activity test.

2.5 X-ray Absorption Spectroscopy (XAS)

2.5.1 X-ray Absorption Near Edge Structure (XANES)

X-ray Absorption Near Edge Structure (XANES) experiment was divided into two parts; ex-situ and in-situ XANES experiments. The ex-situ XANES experiment was conducted to investigate the oxidation state of Ni and Ti on the fresh catalysts. While in-situ experiment was used to monitor the electronic state changing of Ni and Ti during CO_2 methanation. The ex-situ XANES experiment was carried out on beamline 5.2 at Synchrotron Light Research Institute (SLRI), Nakhon Ratchasima, Thailand [20,21]. The Ge (220) was used as double crystal monochromator with energy resolution of 2×10^{-4} eV. The in-situ XANES experiment was carried out on beamline 2.2 at Synchrotron Light Research Institute (SLRI), Nakhon Ratchasima, Thailand. The Si (111) crystal was used as an Energy Dispersive Monochromator (EDM) which covered photons energy of 2400-12000 eV. The linear image sensor was a detector. Samples were prepared by mixing with Boron Nitride (BN) to a homogeneous powder by using ball milling for 20 minutes. After that, the mixed solid sample

was compressed to a pellet. For ex-situ XANES experiment the pellet was placed on a Kapton tape which was stuck on the sample frame. The XANES spectra were collected in the K absorption edge energy for both Ni and Ti in transition mode. The ionization chamber was employed as a detector which was located in front of and behind the sample. For in-situ XANES experiment, the prepared sample in pellet form was placed in an in-situ cell. The in-situ XANES experiment condition was almost the same as CO_2 methanation catalytic activity test. The sample was pretreated with H_2 (24 mL min^{-1}) during the temperature rose up from room temperature to 450 °C (heating rate of 5 °C min^{-1}) and the XAS data were collected for each 10 °C increment. The reduction temperature (450 °C) was held for 1.5 h and the data was also recorded every 10 minutes. After pretreatment, the system was cooled down to 150 °C while the mixed feed gas between CO_2 (6 mL min^{-1}) and H_2 (24 mL min^{-1}) were purged through the sample to start the CO_2 methanation. At the starting state (150 °C), the reaction temperature was raised with the rate of 5 °C min^{-1} to 200 °C and the data was recorded every 10 °C increment. Then, the temperature was kept constant at 200 °C for 20 minutes with recording of the data for every 10 minutes. The experiment was continuously conducted with the same procedure as above; i.e. the reaction temperature was also increased for each 50 °C with the heating rate of 5 °C min^{-1} (recording data for each 10 °C increment) and held at that temperature for 20 minutes (recoding data for each 10 minutes). The reaction temperature of an in-situ experiment was in the range of 150-550 °C. Figure 2 shows the schematic of in-situ experiment for XANES.

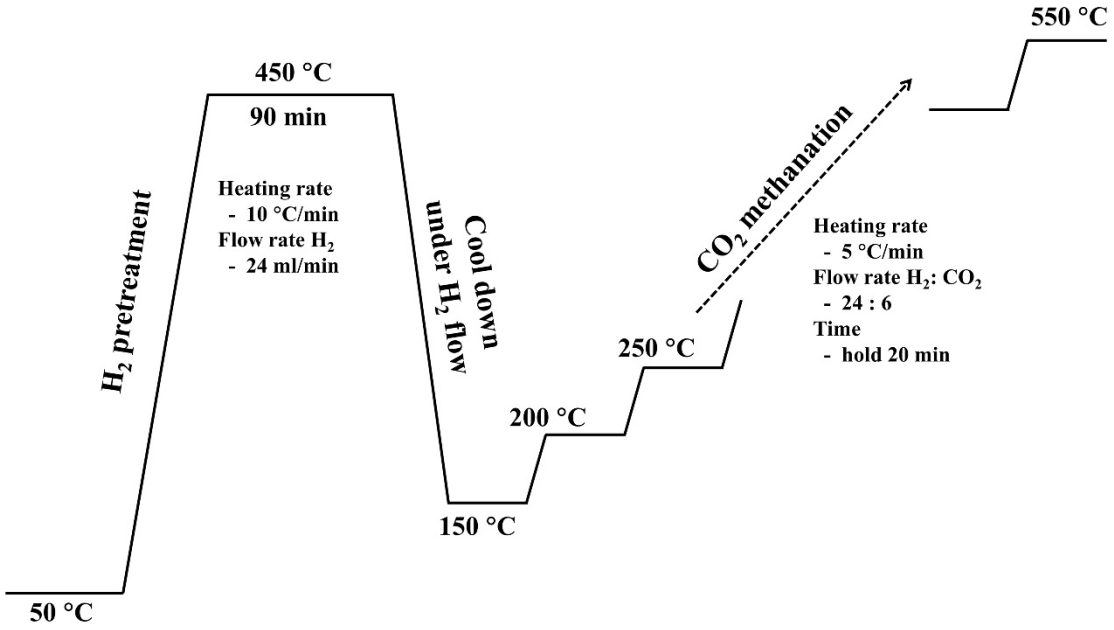

248 **Figure 2** Schematic of in-situ experiment for XANES.

249 **2.5.2 Extended X-ray Absorption Fine Structure (EXAFS)**

250 Extended X-ray Absorption Fine Structure (EXAFS) was carried out to
251 determine the coordination number, interatomic distance and structural and thermal disorder
252 around Ni probe. The EXAFS was used to monitor the electronic state changing of Ni during
253 CO_2 methanation. The experiment was done on Beamline 5.2 at the Synchrotron Light
254 Research Institute (SLRI). (electron energy of 1.2 GeV; bending magnet; beam current 80-150
255 mA; 1.1 to 1.7 x 10^{11} photon s^{-1}). The Ni K-edge experiment was collected in transmission
256 mode (8333 eV). The X-ray incident and transmitted beam intensities were detected by
257 ionization chamber which was placed in front of and behind the sample. Samples were mixed
258 with Boron Nitride (BN) to form a homogeneous powder and compressed to a pellet. The
259 sample was pretreatment under H_2 flowing at 450 °C (20 mL min^{-1}). The pretreatment
260 temperature was hold at this point for 90 min and the data were collected during this state.
261 Afterwards, the system was cooled down to 100 °C and CO_2 was purged at 5 mL min^{-1} to start
262 the reaction. In each step, the reaction temperature was increased for each 50 °C and kept
263 constant for 30 min with collecting the EXAFS spectra. The experiment was continuously run
264 by increasing reaction temperature from 100 to 550 °C.

265 The fine structure of EXAFS region is expressed in terms; $\chi(E)=\mu(E)-$
266 $\mu_0(E)/\Delta\mu_0(E)$, where $\mu(E)$ is the absorption coefficient, $\mu_0(E)$ is the smooth background

function and $\Delta\mu_0$ is the absorption edge. The wave behavior of photoelectron (k) can be written by X-ray energy as; $k=\sqrt{2m_e(E-E_0)/h^2}$, where E_0 is the absorption edge energy and m_e is the electron mass. The oscillation in $\chi(k)$ model of EXAFS region is corresponding to

$$\chi(k)=\sum_j \frac{N_j S_0^2 f_j(k) e^{-2R_j/\lambda} e^{-2k^2\sigma_j^2}}{kR_j^2} \sin\left[2kR_j+\delta_j(k)\right] \quad (9)$$

where N_j is the number of neighboring atoms, R_j is the neighboring distance and σ_j^2 is the disorder of neighboring distance. F(k) and $\delta(k)$ are the scattering-amplitude and phase-shift. S_0^2 is the amplitude reduction factor. The data is usually expressed by Fourier transformation from $\chi(k)$ to R space to study local structure around neighboring atom as

$$\chi(R)=\frac{1}{\sqrt{2\pi}}\int_{k_{min}}^{k_{max}} k^n \chi(k) W(k) e^{i2kR} dk \quad (10)$$

The next step is normalization of the experiment data by ATHENA program. The spectra were amplified by k^2 weight with window in R space range of 1-5 Å and k range of 3-10 $Å^{-1}$. To determine the local structure of Ni-loaded TiO_2 in CO_2 methanation, Ni foil was used as a model fitting of EXAFS data. The experimental EXAFS data was fitted by ARTEMIS program.

3. Results and discussion

3.1 Catalytic performances of CO_2 methanation

The CO_2 methanation was carried out at reaction temperature range of 100-550 °C with a weight hourly space velocity (WHSV) of 48,000 mL g^{-1} h^{-1}. Catalytic performances of TiO_2, 3, 6, 12 and 20wt% of Ni-loaded TiO_2 samples were displayed in term of CO_2 conversion as a function of temperature. The CO_2 conversion, products (CH_4 and CO) selectivities and yields are represented in Figure 3(a)-3(e). The CO_2 conversion for all samples increased according to reaction temperature. However, upon the addition of Ni onto TiO_2, shifting of CO_2 conversion toward lower reaction temperature were observed. For bare TiO_2, the catalytic performance was almost inactive with illustrating of the lowest CO_2 conversion and low CH_4 yield and selectivity, while CO selectivity was relatively high. In contrast, Ni supported TiO_2 catalysts (3, 6, 12 and 20wt% Ni/TiO_2) exhibited a dramatically enhance in catalytic activities which can be observed by increasing of CO_2 conversion at lower reaction temperature. Upon addition of Ni, product selectivities were changed, i.e., CH_4 yield were developed and selectivity toward CH_4 were almost 100%, while CO yield and selectivity were rapidly dropped to lower 10%. This result indicated that addition of Ni onto TiO_2 support improved the desired

product (CH_4) selectivity and suppressed an unwanted product (CO). Increase of Ni concentration resulted in increasing of CO_2 conversion and CH_4 yield, while CH_4 selectivities were almost nearly the same (~100%) for all samples. However, 20wt% Ni/TiO_2 exhibited the highest CO_2 conversion and CH_4 yield, it is noteworthy that the CH_4 selectivity was almost 100% in the wide range of reaction temperature (150-450 °C).

In order to study the kinetic parameter (apparent activation energy), heat and mass transfer effects were checked during measurement of reaction rate by the Koros-Nowak test [22]. The catalytic performances were tested by using samples with different of Ni active site loading (6wt% and 20wt% Ni) at 250 °C at feed gas ratio of $H_2/CO_2/He$ = 24:6:10 and WHSV = 48,000 mL g^{-1} h^{-1}. The results revealed that the CO_2 conversion of 6wt% Ni/TiO_2 and 20wt% Ni/TiO_2 were 1.90 and 4.30 %, respectively, while turn over frequency (TOF) were almost the same values (0.27 s^{-1} and 0.25 s^{-1}, respectively). Therefore, it was attributed that heat and mass transfer were absence for this experiment condition.

The apparent activation energy (E_a) was usually used to elucidate the catalytic performance in enhancing the reaction rate. This value can be obtained by using the Arrhenius equation ($k = Ae^{-E_a/RT}$). The plotting between ln(rate) and reciprocal of absolute temperature (1/T) was constructed. The slope of the linear graph was used to calculate the apparent activation energy. Figure 4 illustrates the Arrhenius plots of 3, 6, 12 and 20wt% Ni/TiO_2. It was seen that the apparent activation energies were decreased with increasing of Ni content (E_a ranges between 68-78 kJ mol^{-1}). Reduction of apparent activation energy upon more Ni addition indicated that lower kinetic barrier for catalyzing toward the reaction, thus, the catalytic activity can be enhanced. The E_a values were corresponded to the catalytic activities results that 20wt% Ni/TiO_2 exhibited the highest CO_2 conversion due to the lowest E_a for this reaction. The long-term stability test is also an important property to determine the efficiency of catalyst in thermal sintering for industrial scale. Figure 5 exhibits the CO_2 conversion and CH_4 yield of 20wt% Ni/TiO_2 in CO_2 methanation for 72 h. The stability test of 20wt% Ni/TiO_2 was done by keeping the reaction temperature at 420 °C since this temperature exhibited the highest in CO_2 conversion. The CO_2 conversion was stable during 72 h on stream (decrease

not over 10%) which was corresponded to consistency of CH_4 selectivity (almost 100%) for this sample.

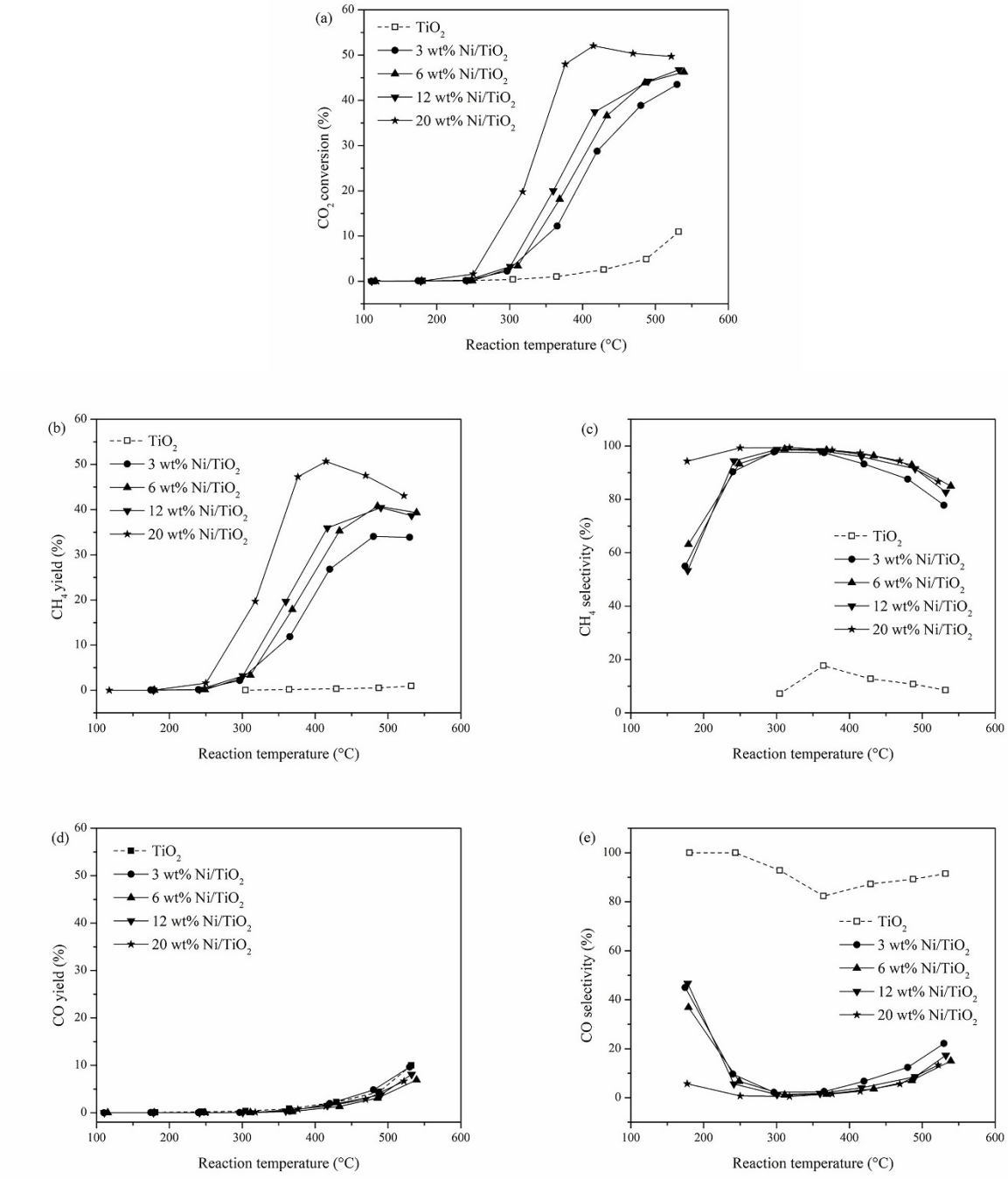

Figure 3 (a) CO_2 conversion, (b) CH_4 yield, (c) CH_4 selectivity, (d) CO yield and (e) CO selectivity of all catalysts; TiO_2, 3, 6, 12 and 20wt% Ni-loaded TiO_2 by using $H_2/CO_2/He$ = 24:6:10, total flow rate 40 mL min^{-1}, WHSV = 48,000 mL g^{-1} h^{-1} at reaction temperature 100-550 °C.

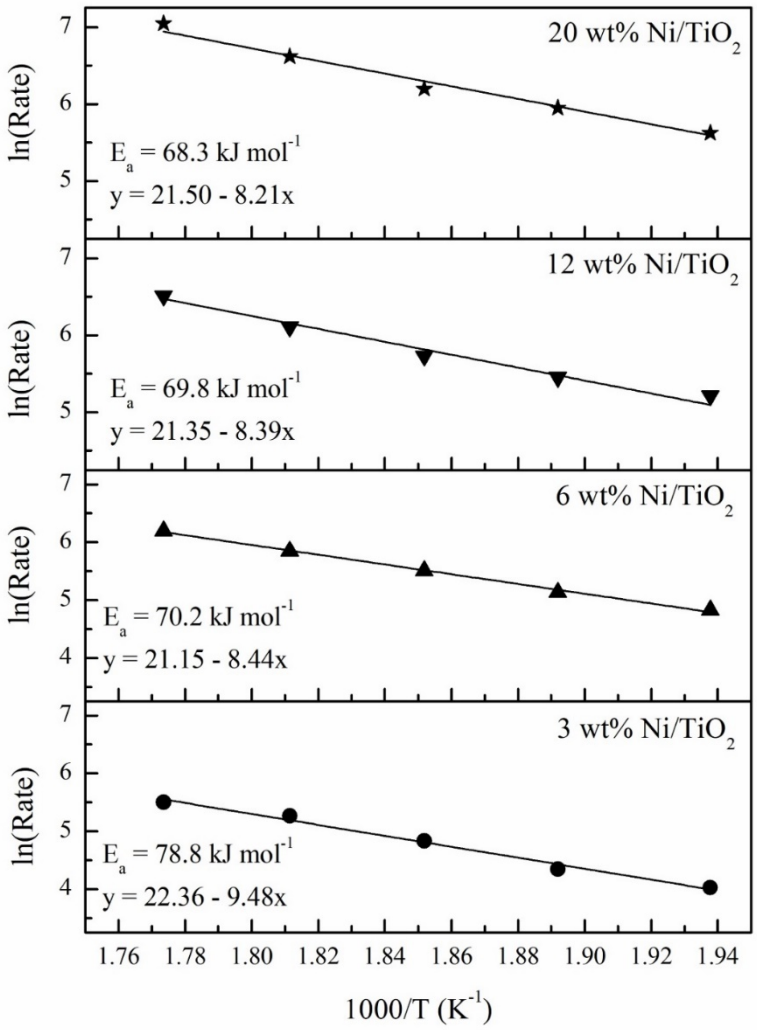

Figure 4 Arrhenius plots for the CO_2 methanation with different Ni contents on TiO_2; TiO_2, 3, 6, 12 and 20wt% Ni/ TiO_2.

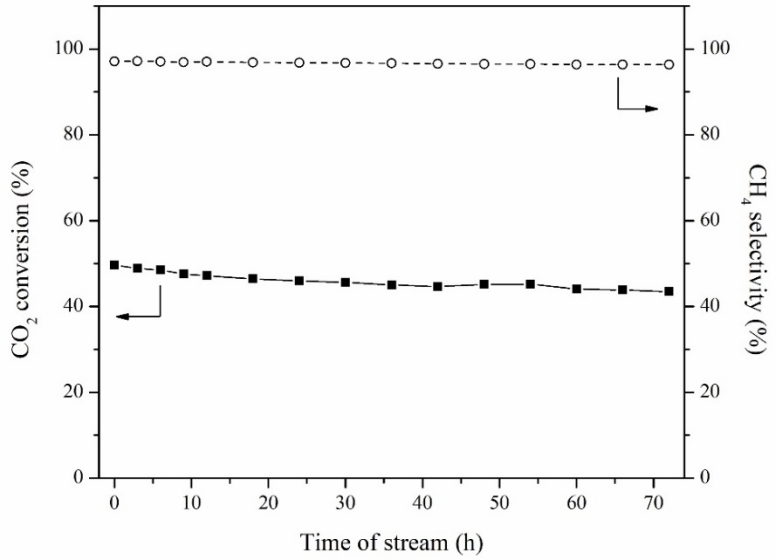

Figure 5 CO_2 conversion and CH_4 selectivity over 20wt% Ni/ TiO_2 during long-term stability test at reaction temperature of 420 °C, $H_2/CO_2/He$ = 24:6:10 and WHSV = 48,000 mL g^{-1} h^{-1}.

3.2 Standard characterization

3.2.1 X-ray diffraction (XRD)

XRD patterns of TiO_2 with various Ni contents (3, 6, 12 and 20wt%) are shown in Figure 6. The XRD peaks of TiO_2 were observed at 25.3°, 37.8 °, 48.0°, 53.9°, 55.1, 62.7, 68.9°, 70.3° and 75.1° which were corresponding to (101), (004), (200), (105), (211), (204), (110), (220) and (215) planes of anatase structure with using JICST database (from The Crystallographic Society of Japan). For all Ni-loaded catalysts (3, 6, 12 and 20wt%), the anatase structure of TiO_2 remained unchanged. However, the intense diffraction peaks decreased when increasing of Ni loading. The lowering of these peaks related to reducing of crystallinities and crystalline sizes of TiO_2. This indicated that addition of Ni into TiO_2 during sol-gel process can prevent the crystalline growth of TiO_2 [23]. It was found that the crystalline sizes of TiO_2 were reduced with more added of Ni content as illustrated in Table 1. In addition, shifting of diffraction peaks to lower diffraction angles were also observed which indicated to unit cell expansion. This phenomenon resulted from the substitution of Ti^{4+} ion by larger Ni^{2+} ion (ionic radii of Ni^{2+} = 0.72 Å and Ti^{4+} = 0.68 Å for 6-fold coordination). The unit cell of TiO_2 catalyst was enlarged upon increase of Ni content which indicated to more incorporation of Ni^{2+} ions into TiO_2 lattice [24-26]. To confirm the incorporation of adding metal into host lattice, the Williamson-Hall (W-H) parameter was used. Upon incorporation of adding metal,

the host lattice was distorted and strain was increased. In this case, Ti^{4+} site was replaced by Ni^{2+} divalent cation, thus oxygen vacancies were expected to form. Therefore, the W-H parameter can indicate to the degree of incorporation of adding metal [27,28]. Table 1 summarizes the unit cell parameter, unit cell volume and lattice strain of all synthesized samples. It can be seen that the unit cell parameter and unit cell volume were increased with increasing of Ni loading. The lattice strain was also enlarged which indicated to higher amount of incorporated Ni^{2+} into TiO_2 lattice upon increase of Ni content.

Besides the TiO_2 anatase diffraction peaks, another additional important peak was also observed, i.e., NiO diffraction peak at 43.5°. This peak was attributed to a face centered-cubic crystalline structure of NiO. It was noteworthy that this peak was not observed in the low Ni content sample (3wt% Ni/TiO_2). This was probably due to completely incorporate of adding Ni ion into TiO_2 and the solid solution was formed. In contrast, the NiO diffraction peak was obviously appeared for Ni loading $\geq$ 6wt%. This result can imply that addition of Ni was existed in two forms, i.e., incorporation of Ni ion into TiO_2 lattice and dispersion of NiO onto TiO_2 surface. Therefore, there was a limitation or saturated level of incorporation of Ni ion into TiO_2 lattice and then the excess of Ni added amount can disperse onto TiO_2 surface. From this behavior, both shifting of XRD peaks and existing of NiO peak were observed. In order to estimate the saturated value of Ni concentration, the relationship between unit cell volume and Ni content was constructed as illustrated in Figure 7. It can be seen that the unit cell volume was increased upon addition of Ni and the expansion of lattice was almost constant at higher Ni loading more than 6wt%. Form this plot, the saturated Ni incorporated amount was in the range between 3-6wt%. Therefore, from our results, we assumed that the saturated Ni incorporated amount was 3wt% which mean that all Ni addition was incorporated into TiO_2 lattice at this added level. Increasing of Ni content at higher amount than 6wt%, the excess amount of adding Ni was dispersed onto TiO_2 surface and more intense of NiO diffraction peak was observed which indicated to higher crystallinity and crystalline size of NiO phase. To evidence the substitution of Ni ion into TiO_2 lattice and dispersion of NiO phase onto catalyst surface, X-ray Absorption Spectroscopy (XAS) results were used and discussed in the next part.

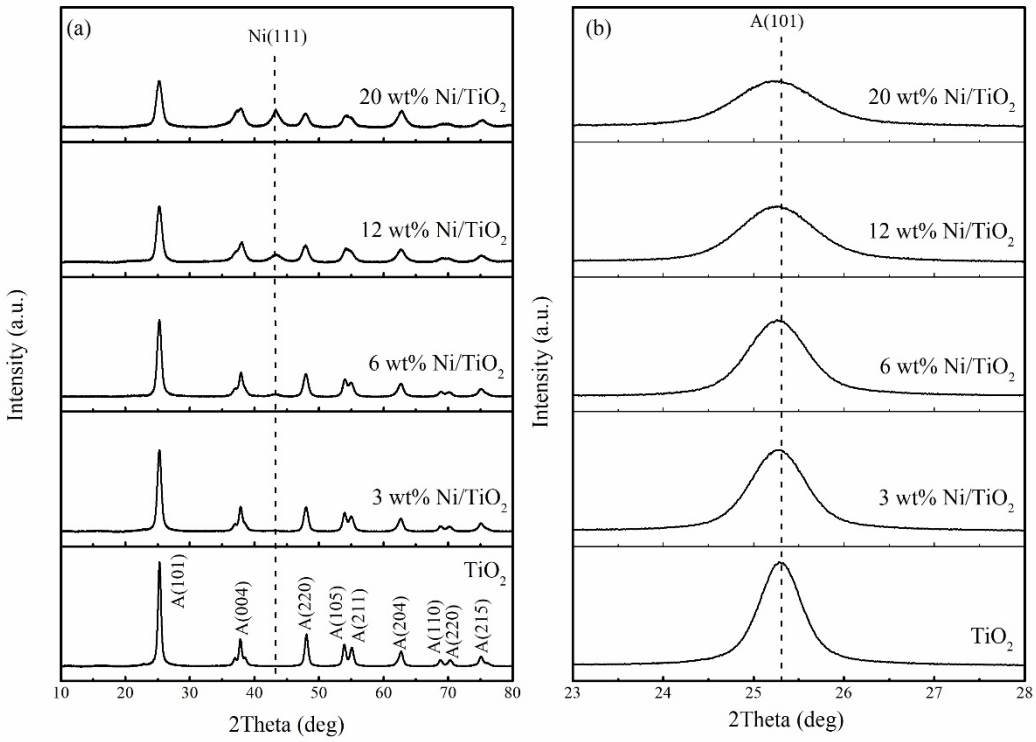

386 **Figure 6** (a) XRD diffraction patterns of all catalysts.

387 (b) magnification of (101) crystallographic plane for all catalysts to compare

388 the shifting of the diffraction peak.

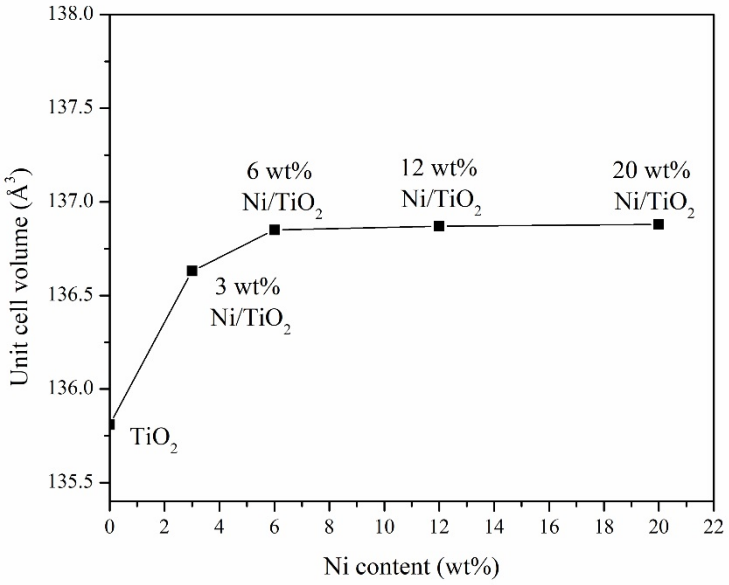

389 **Figure 7** Relationship between unit cell parameters of all catalysts against Ni content.

390

Table 1 Structural and physical properties of all synthesized samples including lattice parameter, cell volume, crystal size, lattice strain and Ni content.

Samples	Lattice parameter[a] (Å)		Cell volume[a] ($Å^3$)	Crystal size[b] (nm)		Lattice strain[c]	Ni contents[d] (wt%)
	a = b	c		Anatase	Ni		
TiO_2	3.778	9.516	135.81	14.92	-	3.65×10^{-4}	-
3wt% Ni/TiO_2	3.791	9.506	136.63	11.41	3.99	7.35×10^{-4}	2.92
6wt% Ni/TiO_2	3.793	9.501	136.85	10.63	4.55	1.66×10^{-3}	6.07
12wt% Ni/TiO_2	3.801	9.475	136.87	8.37	3.98	4.03×10^{-3}	13.5
20wt% Ni/TiO_2	3.780	9.483	136.88	7.84	5.31	7.83×10^{-3}	21.5

[a]Calculated from the plane (101), (004), (100) by Bragg's equation.

[b]Calculated from the plane (101) for anatase and (111) for Ni using Scherer's equation.

[c]Calculated from Williamson-Hall (W-H).

[d]Calculated from ICP-OES results.

3.2.2 Structural study of Ni-loaded TiO_2 catalysts by X-ray Absorption Spectroscopy (XAS)

As discussed above that there were two forms of Ni addition; Ni substitution and NiO dispersion, thus in this part, X-ray Absorption Spectroscopy (XAS) results were used to evidence the existing of these two forms. The first form, substituted of Ni ion into TiO_2, Extended X-ray Absorption Fine Structure (EXAFS) of 3wt% Ni/TiO_2 was analyzed and discussed to confirm the substitution of Ni ion into TiO_2 lattice. Another form, dispersed NiO, linear combination between substitution Ni and NiO was performed and then the percentage composition of substitution Ni and NiO were determined.

For Ni substitution form, analysis of EXAFS result of 3wt% Ni/TiO_2 was used since we assumed the complete substitution of all added Ni amount for this sample. The Ti K-edge EXAFS oscillation spectra and Fourier transformed functions for TiO_2 and 3wt% Ni/TiO_2 by using anatase TiO_2 (space group $I4_1/amd$) as a model for fitting are shown in Figure 8. For Ni-loaded TiO_2 sample, the FT-EXAFS spectra were obtained by fitting with anatase TiO_2 and replacing one atom of the nearest Ti atom with Ni. The k^2-weighted Fourier transform was used (Figure 8(a)). The weight EXAFS data in k space was in the range from 3-10 $Å^{-1}$ and was transformed to R space without phase collection (Figure 8(b)). The structural parameters of TiO_2 and 3wt% Ni/TiO_2 for Ti K-edge are summarized in Table 2. For Figure 8(b), the sharp peak of TiO_2 at ~1.5 Å was referred to the oscillation of Ti–O in the first shell. Upon

incorporation of Ni in second shell of TiO_2 lattice, the Ti–O bond distance were distorted (as shown in Table 2), while the Ti–Ni bond length was elongated due to substitution by larger cation and then resulted in shortening of Ti–Ti bond distance.

From the results of XRD, it can be seen that both Ni incorporated and dispersed phase of NiO were observed, especially for high Ni content than 6wt%. In order to determine the compositions of these two forms of Ni species, linear combination of XANES spectra were employed. For this approach, we assumed that all Ni loading at 3wt% was completely substituted into TiO_2 lattice, thus the excess amount of added Ni (higher than 3wt%) was existed in NiO dispersed form. Therefore, the linear combination between substituted Ni and dispersed NiO was constructed and was used as a standard to estimate the composition between two forms of Ni species. For this work, Ni K-edge XANES spectrum of 3wt% Ni/TiO_2 was used as a standard for Ni substitution while that of NiO was used as a standard for NiO dispersion phase. Figure 9 displays the percentage of two forms of Ni species obtained from linear combination fitting. It was seen that NiO phase increased with Ni content which was corresponding to XRD results.

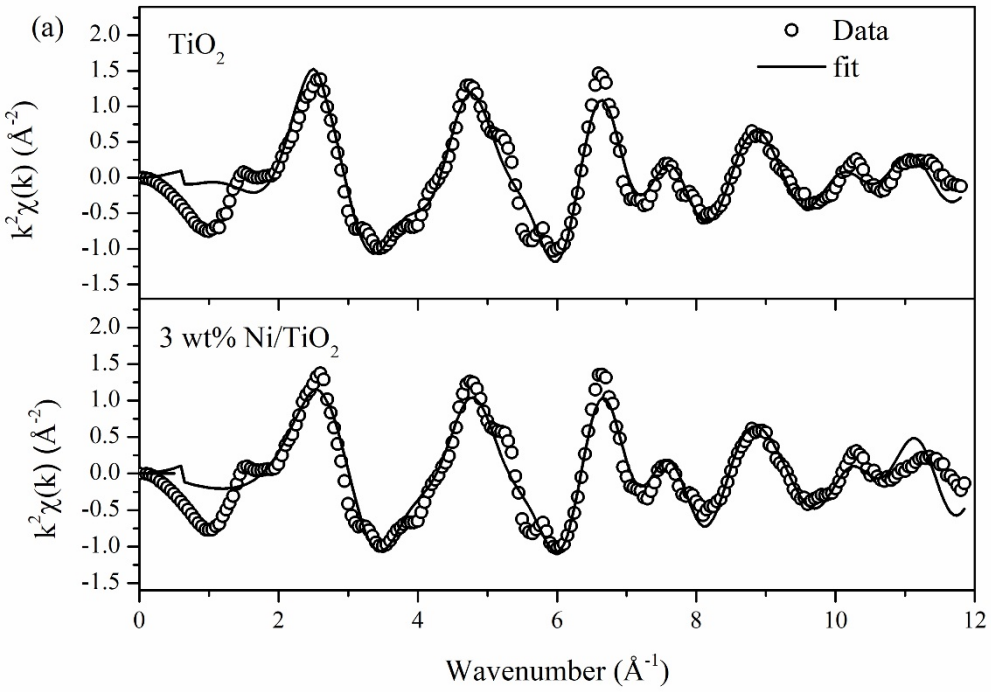

Figure 8 (a) Ti K-edge EXAFS oscillation data with $k^2\chi(k)$ for TiO_2 and 3wt% Ni/TiO_2.

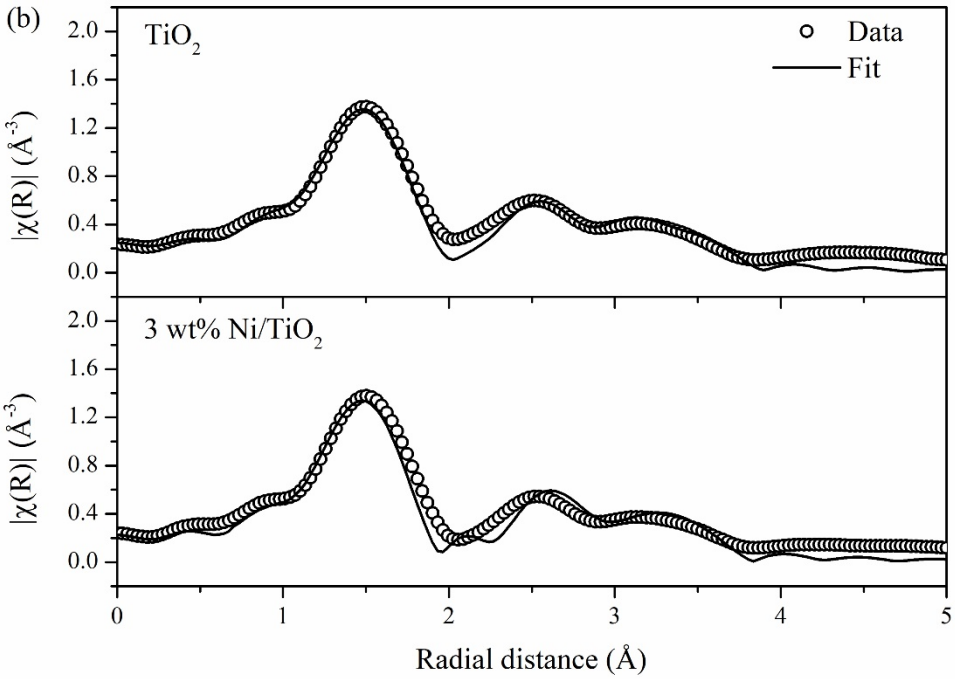

Figure 8 (b) Fourier transform data of Ti K-edge EXAFS for TiO_2 and 3wt% Ni/TiO_2.

Table 2 Structural parameter for Ti K-edge EXAFS fitting analysis.

Samples	Shells	Best fit EXAFS parameters			
		N	σ^2	ΔE (eV)	R (Å)
TiO_2	Ti-O	2.3	0.003	1.439	1.908
	Ti-O	1.2	0.001		1.996
	Ti-Ti	2.3	0.007		3.088
3wt% Ni/TiO_2	Ti-O	1.9	0.001	1.474	1.927
	Ti-O	0.9	0.003		1.947
	Ti-Ti	1.4	0.002		3.051
	Ti-Ni	0.5	0.003		3.291

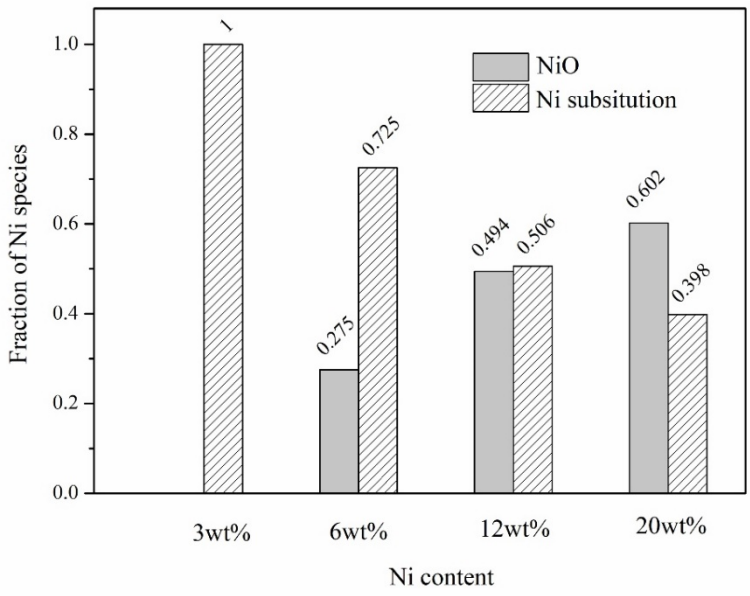

Figure 9 The comparison between Ni substitution amount and NiO phase of all Ni-loaded catalysts which obtained from comparing to a linear combination of XANES data of Ni K-edge between 3wt% Ni/TiO_2 and NiO.

3.2.3 Surface and physical properties of catalysts

The surface properties of TiO_2 and modified-TiO_2 catalysts were estimated by N_2 adsorption-desorption technique. The N_2 adsorption-desorption isotherms are displayed in Figure 10. All isotherms exhibited an adsorption-desorption feature corresponded to mesoporous materials. The surface area, pore size and pore volume of samples are summarized in Table 3. The BET surface area of pure TiO_2 was 72 m^2/g with pore volume of 0.15 cm^3/g. The Ni modified TiO_2 samples exhibited higher BET surface area and pore volume than that of original TiO_2 upon increasing of Ni addition amount. The surface area of 3, 6, 12 and 20wt% Ni/TiO_2 were ca. 92, 95, 100 and 108 m^2/g, respectively. These results were in agreement with XRD analysis which mentioned the prevention of anatase crystal growth by Ni addition and led to lowering of TiO_2 crystalline sizes. Higher surface area was important to improve the active surface sites to adsorb gas substrates for CO_2 methanation [29]. The pore size distributions of the synthesized samples were in the range of 2-16 nm (inset). The pore diameter distributions of TiO_2 and 3wt% Ni/TiO_2 gained the maximum value at 9 nm whereas higher Ni contents samples (6, 12 and 20wt% Ni/TiO_2) provided the smaller of diameter at a maximum peak around 6 nm. Pore volumes of Ni-added samples were higher than that of pure TiO_2.

The percentage of added Ni content in all Ni-loaded catalysts were determined by inductively couple plasma-optical emission spectroscopy and the results are summarized in Table 1. The obtained results of Ni content from ICP-OES in all Ni-loaded catalysts exhibited a similar value to nominated added amount (2.92, 6.07, 13.5 and 21.5wt% Ni for 3, 6, 12 and 20wt% Ni/TiO_2, respectively).

The morphology of fresh TiO_2 and Ni supported TiO_2 are showed in Figure 11(a-e). The shape of particles for all samples were uniformly spherical and there was no change of the anatase morphology for all Ni catalysts. The means of anatase particle sizes were approximately in the range of 8-15 nm and the particle sizes were decreased upon increasing of Ni content which was in agreement with XRD results. NiO was characterized using high-resolution TEM for 20wt% Ni/TiO_2 resulting in Figure 11(f). The detection of lattice spacing 0.210 nm can be indexed as (200) plane of FCC Ni which were related to XRD patterns. This result was confirmed the existence and dispersion of NiO.

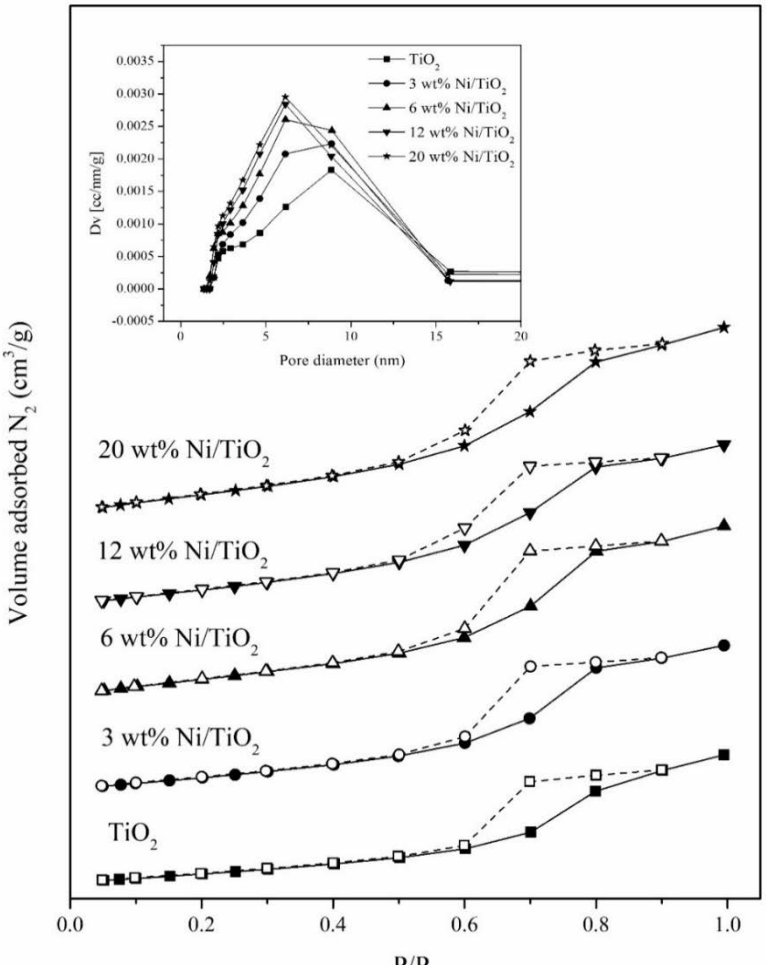

Figure 10 N_2 adsorption-desorption isotherms and pore size distribution (inset) of all catalysts; TiO_2, 3, 6, 12 and 20wt% Ni-loaded TiO_2. Solid symbol is adsorption branch and open symbol is desorption branch.

487 **Table 3** Surface properties of samples (TiO_2, 3, 6, 12 and 20wt% Ni/TiO_2).

Samples	Surface area[a] (m^2/g)	Pore volume[a] (cm^3/g)	Pore size[a] (nm)	H_2 consumption[b] (mmol/g)	H_2 chemisorbed[c] (μmol/g)
TiO_2	71.48	0.1490	8.340	-	-
3wt% Ni/TiO_2	91.80	0.1743	7.596	13.9	5.8
6wt% Ni/TiO_2	95.41	0.1776	7.745	31.1	13.8
12wt% Ni/TiO_2	100.3	0.1749	6.947	62.5	25.5
20wt% Ni/TiO_2	107.6	0.1934	7.191	76.2	43.4

[a]Estimated from N_2 adsorption-desorption.

[b]Estimated from H_2-TPR.

[c]Estimated from H_2 chemisorption.

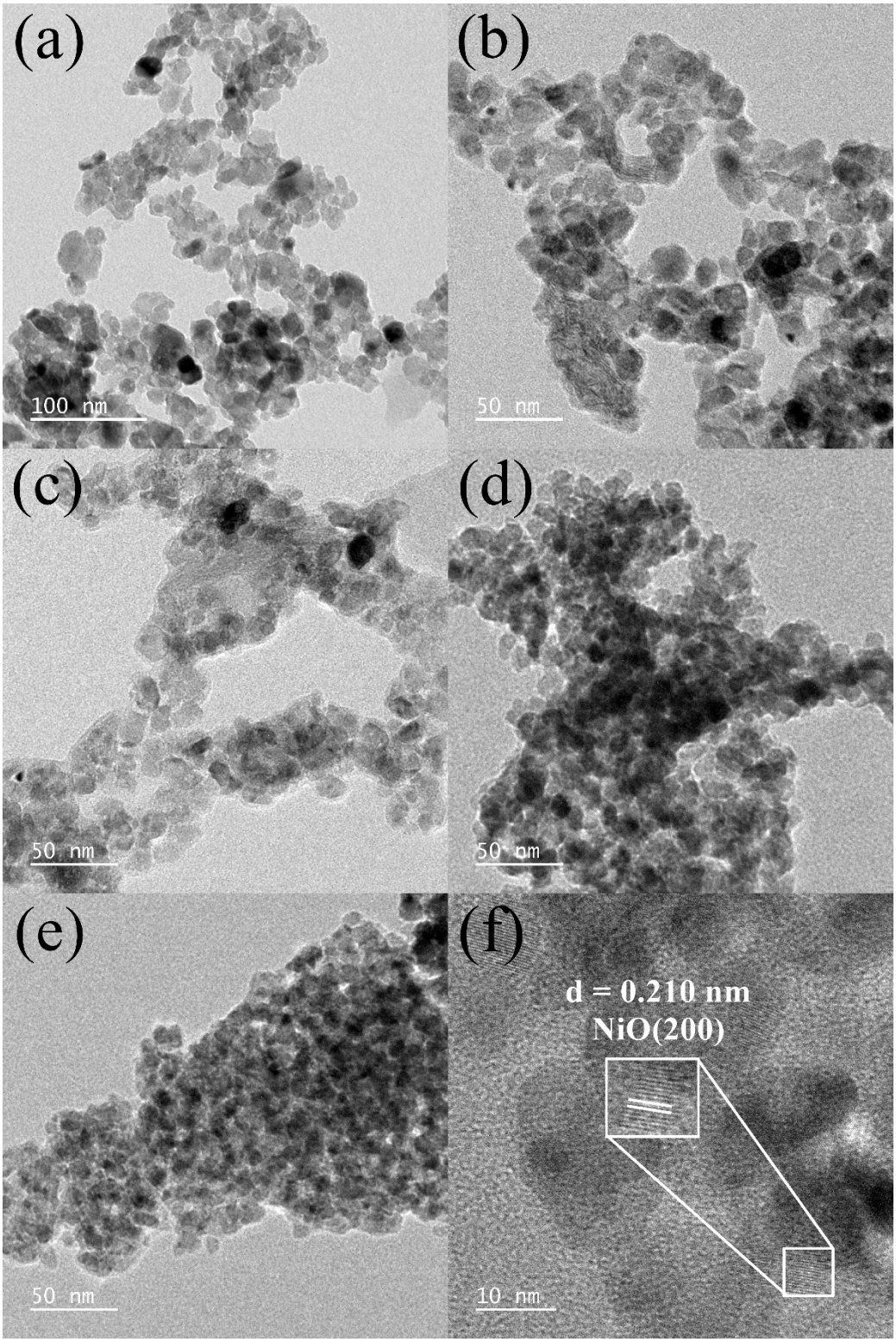

488 **Figure 11** TEM images of (a) TiO_2, (b) 3, (c) 6, (d) 12, (e) 20wt % Ni-loaded TiO_2 and
489 (f) HRTEM for 20wt % Ni-loaded TiO_2.

490

491

3.3.3 H_2 Temperature Program Reduction (H_2-TPR) and H_2 chemisorption

H_2 Temperature Program Reduction (H_2-TPR) is attributed to the interaction of metal active site and support. Figure 12 demonstrates the TPR profiles of 3, 6, 12 and 20wt% Ni-loaded TiO_2 catalysts. The reduction peaks were observed in the range of 250-450 °C which were assigned as conversion of Ni^{2+} to Ni^0 on surface which interacted with TiO_2 support [30,31]. The different reduction temperature of NiO was attributed to different degree of interaction between NiO and TiO_2 support. This behavior depended on the preparation method and calcination temperature since these factors caused a different NiO dispersion state, NiO sizes and degree of interaction with TiO_2 and thus resulted in different reducibility of NiO particles. The shifting of NiO reduction peaks to higher temperature were observed upon increasing of Ni content which indicated to high dispersion of NiO species with stronger interaction with TiO_2 support [32]. Moreover, H_2 consumption considerably enhanced with the increase of Ni additions as follows: 3 < 6 < 12 < 20wt% Ni/TiO_2 as shown in Table 3. The signal of H_2-TPR is referred to the amount of H_2 consumption, i.e., more intense of reduction peak implies to high H_2 consumption to reduce the metal in a catalyst. It was clearly seen that H_2 consumption was related to amount of NiO phase reduction to Ni metal; 20wt% Ni-modified TiO_2 provided 76.2 mmol/g of H_2 which was 5.5 times higher that H_2 consumption of 3wt% Ni-modified TiO_2.

In order to validate the exposed NiO and/or Ni active species on catalyst surface, H_2-chemisorption experiment was conducted. Due to H_2 favor to adsorb on metal active site, thus higher amount of H_2 chemisorbed can indicate to higher amount of metal active site. Table 3 illustrates the amount of H_2 chemisorbed of all catalysts. It is seen that the H_2 chemisorbed amount was increased with increasing of Ni loading on catalyst surface which corresponded to higher area of Ni adsorption sites for H_2. Since H_2 is one of the reactants for CO_2 methanation, thus the results of H_2 chemisorption was related to enhance of catalytic activities of Ni-loaded catalysts which will be discussed in the latter part.

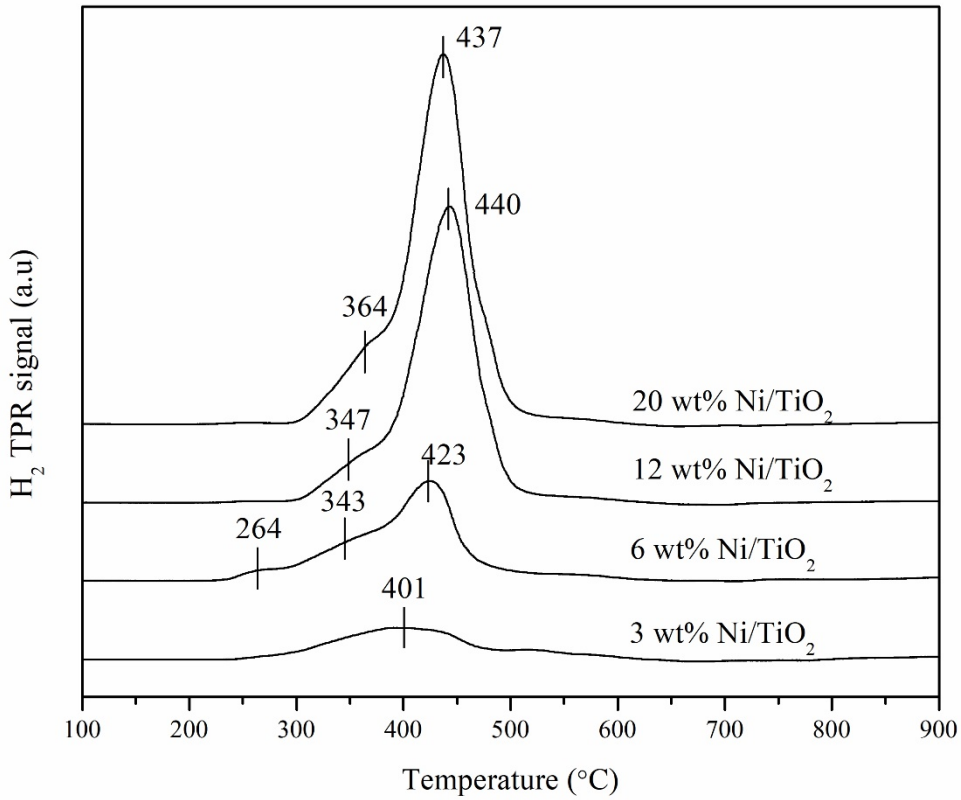

Figure 12 H_2 TPR profiles of TiO_2, 3, 6, 12 and 20wt% Ni-loaded TiO_2.

3.3 X-ray Absorption Spectroscopy analysis

From catalytic activities results, it was found that addition of Ni into TiO_2 lattice led to structural, physical and redox properties changing which also evidenced the altering of catalytic activities performance. In this part, X-ray Absorption Spectroscopy (XAS) was used to investigate the electronic state changing of Ni and Ti in freshly prepared catalysts and monitor the changing of the catalysts during CO_2 methanation. The changing of catalysts properties was studied by using data analysis of two regions; X-ray Absorption Near Edge Structure (XANES) and Extended X-ray Absorption Fine Structure (EXAFS). All of data reduction from XAS can be used to understand and describe the effect of Ni addition into TiO_2 in improving CO_2 methanation.

3.3.1 X-ray Absorption Near Edge Structure (XANES) for monitoring Ni and Ti oxidation states

This part is divided into two parts; 1) ex-situ XANES analysis for freshly synthesized catalyst and 2) in-situ XANES analysis for monitoring Ni and Ti oxidation state during CO_2 methanation.

Figure 13(a) illustrates Ni K-edge XANES spectra of all freshly prepared Ni-loaded TiO_2 catalysts compared with Ni foil and NiO standards. The Ni foil spectrum exhibits an edge energy at around 8333 eV which is attributed to the electron transition from 1s to 3d orbital [33]. For NiO standard, the white line peak at 8347 eV was observed which corresponded to multiple scattering process in octahedral NiO [33,34]. The oxidation state of probe atom can be initially estimated by comparing with the standard XANES spectra with certain oxidation state. From Figure 13(a), the Ni XANES spectra of Ni-loaded samples were almost identical to NiO standard spectrum which indicated to oxidation state of Ni-loaded TiO_2 in all samples were 2+. Moreover, in order to elucidate the oxidation state of Ni, the relationship between ΔE (different of edge energy relative with Ni foil) and oxidation state of Ni was constructed. The edge energy of all samples can be obtained by taking the first derivative of those spectra and the turning point was assigned as an edge energy. Figure 13(b) displays the relationship between ΔE and oxidation states of Ni for all Ni-loaded samples compared with two Ni standards. It can be seen that the apparent oxidation states of Ni for all Ni-loaded samples were 2+. Normalized Ti K-edge XANES spectra of all fresh as-synthesized samples display in Figure 14. Characteristic peaks of TiO_2 support and Ni-loaded samples were marked as pre-edge peaks A_1–A_3 and B, a shoulder peak as C and a white line peak as D as shown in Figure 14(a) [35]. The first pre-edge peak (A_1) was corresponding to a quadrupole transition to 3d (t_{2g}) state of the TiO_6 octahedron while that of A_3 and B peaks were assigned as dipole transition from 1s to hybridized p-d state of t_{2g} and e_g, respectively. The A_2 was not noticed in the larger size of anatase and rutile TiO_2, but this peak appeared in the case of the small sized nanostructures [36]. The shoulder C was noted as transition shakedown process while that of D was assigned as transition of 1s to out-of-plane $4p_z$ orbital [37]. The structures of all fresh samples were detected as anatase TiO_2 structure with consisted of Ti^{4+} surrounding with six-fold coordinate which were related to XRD results. It is known that formation of oxygen vacancies within TiO_2 lattice lead to change of Ti^{4+} oxidation state to Ti^{3+} and distortion in the local TiO_6 octahedral coordination [38]. In the first change, the changing of Ti^{4+} oxidation state to Ti^{3+} was not observed from our results which might be due to small amount of metal addition when comparing with bulk TiO_2 concentration, thus, the changing of Ti^{3+} was too small. On the other hand, the distortion in TiO_2 octahedral is caused from elongation or shortening of Ti–O bond length. Changing of Ti–O bond length lead to alteration of Ti 3d and O 2p density of state (DOS) and the changing of Ti–O orbital overlap results in changing the total DOS and its corresponding to electronic transition which reflected to the pre-edge feature [39]. The

567 changing of pre-edge feature is usually used to indicate the influence of metal substitution into
568 host lattice. The pre-edge intensities were related to the symmetry of the crystal lattice, thus, a
569 distortion and oxygen vacancies can cause an increase of pre-edge peaks [38-42]. Figure 14(b)
570 shows Ti K-edge in the pre-edge region for TiO_2 and 3wt% Ni/TiO_2 and 20wt% Ni/TiO_2. The
571 pre-edge intensities increased with increasing of Ni content which was attributed to higher
572 distortion and oxygen vacancies formation within TiO_2 lattice. This result can also confirm the
573 substitution of Ni^{2+} ions into Ti^{4+} sites which led to oxygen vacancies formation and distortion
574 of TiO_2 lattice. This phenomenon was in agreement with XRD and Ti EXAFS analysis for
575 3wt% Ni/TiO_2 as discussed in the first part.
576 Second part is in-situ XANES analysis for monitoring Ni and Ti oxidation
577 states during CO_2 methanation. In-situ Time-Resolve X-ray Absorption Spectroscopy (in-situ
578 TR-XAS) was used to obtain the XANES results. 20%wt Ni/TiO_2 synthesized sample
579 performed the highest CO_2 methanation activity, thus, this sample was selected to study by in-
580 situ TR-XAS.
581 The original Ni oxidation state of freshly prepared Ni catalysts was +2
582 which were confirmed by XANES results in previous part. In in-situ experiment, catalyst
583 surface was cleaned up and reduced by using H_2 during heating from 50 to 450 °C as shown in
584 Figure 15(a). During H_2 pretreatment, the characteristic peak of Ni species did not change in
585 the temperature range from 50 to 340 °C. After that, the white line intensity of Ni^{2+} (8347 eV)
586 obviously decreased and then the feature of spectra was slightly changed with increase of
587 pretreatment temperature and completely converted at 450 ˚C. After the temperature reached
588 to 450 ˚C, the pretreatment temperature was hold at this point for 90 min to maintain metallic
589 Ni active species before staring the reaction [43,44]. It indicated that the H_2 pretreatment
590 process resulted in reduction of NiO to Ni^0. Figure 15(b) shows in-situ TR-XAS results of
591 20wt% Ni/TiO_2 during CO_2 methanation with H_2/CO_2 ratio = 4 at reaction temperature range
592 of 150 to 550 °C. The oxidation state of Ni remained unchanged during CO_2 methanation (Ni^0)
593 within the whole range of reaction temperature.
594 Figure 16(a) shows in-situ TR-XAS results of Ti K-edge for 20wt% Ni/TiO_2 over H_2
595 pretreatment condition at 50 to 450 °C. It can be seen that the spectra of 20wt% Ni/TiO_2 under
596 pretreatment condition remained unchanged (Ti^{4+}) and after conducting the CO_2 methanation,
597 the oxidation state of Ti was still unchanged which can be observed by the same spectra feature
598 of Ti K-edge for both pretreatment and reduction process (Figure 16(b)).

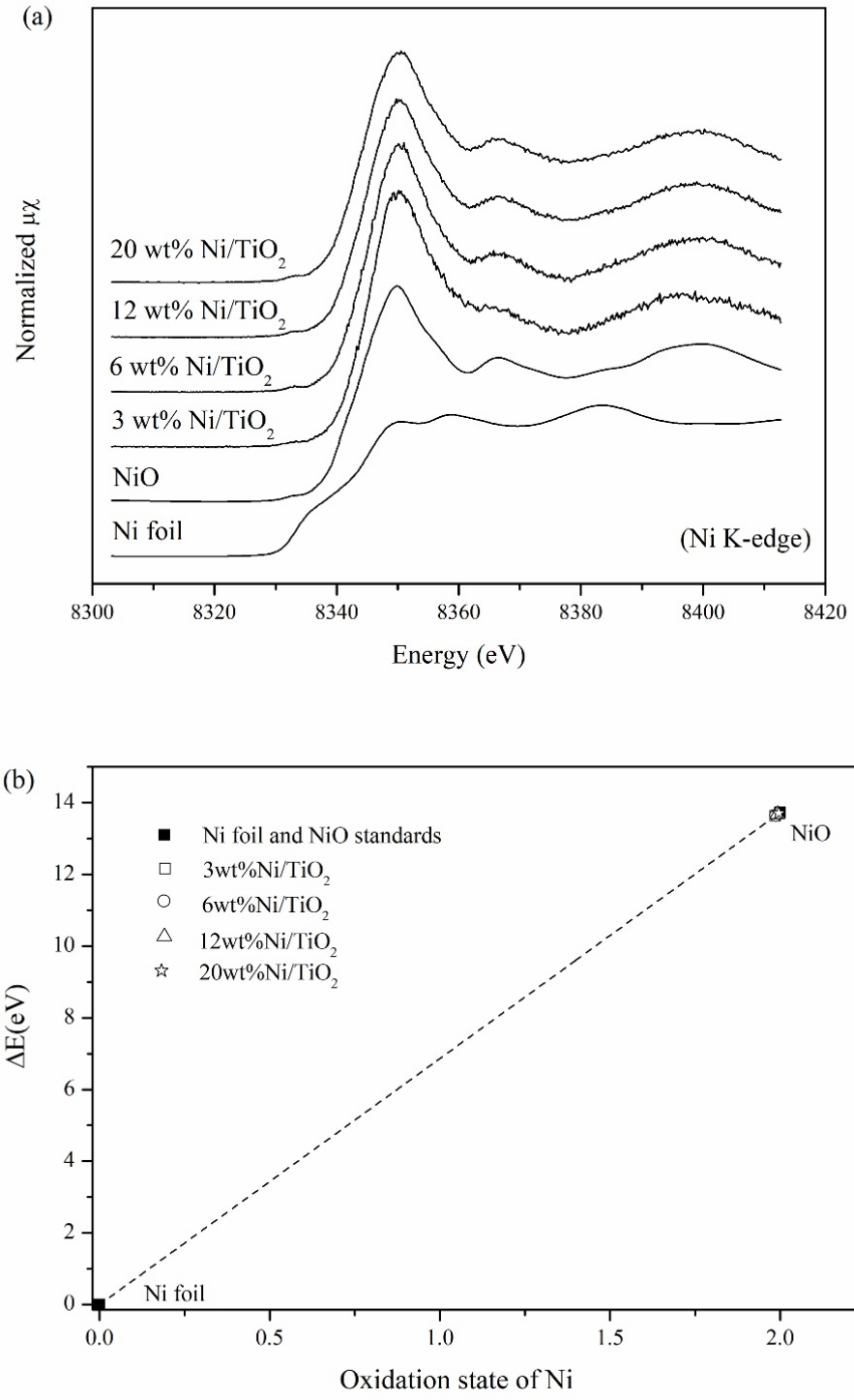

Figure 13 (a) Normalized Ni K-edge XANES spectra of fresh samples (pure TiO_2, 3, 6, 12 and 20wt% Ni/TiO_2) and references (NiO, Ni foil).

(b) Relationship between ΔE and oxidation state of Ni for determining the oxidation state of Ni in all synthesized catalysts.

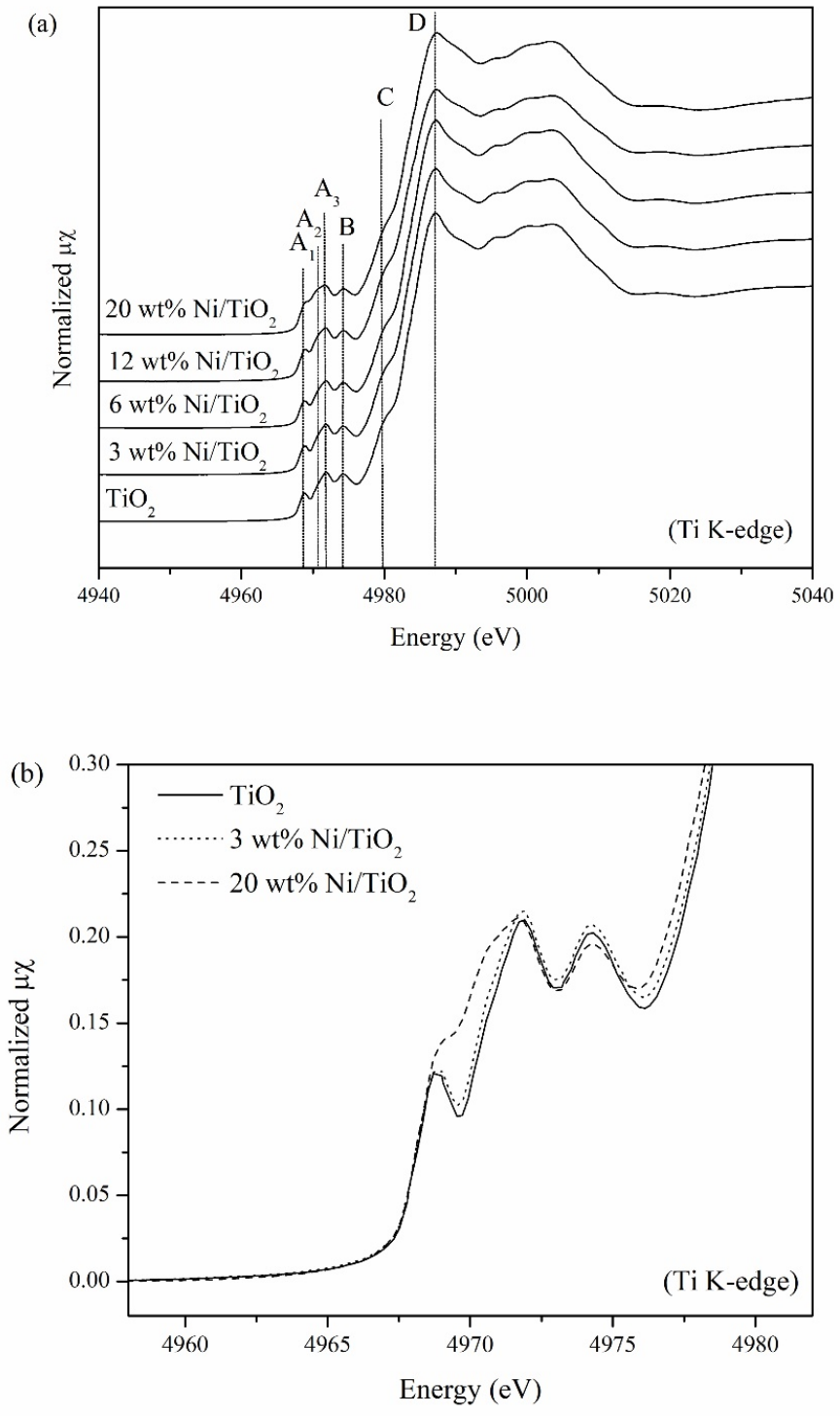

Figure 14 (a) Normalized Ti K-edge XANES spectra of fresh samples (pure TiO_2, 3, 6, 12 and 20wt% Ni/TiO_2).

(b) Ti K-edge XANES spectra in pre-edge region of TiO_2, 3wt% Ni/TiO_2 and 20wt% Ni/TiO_2.

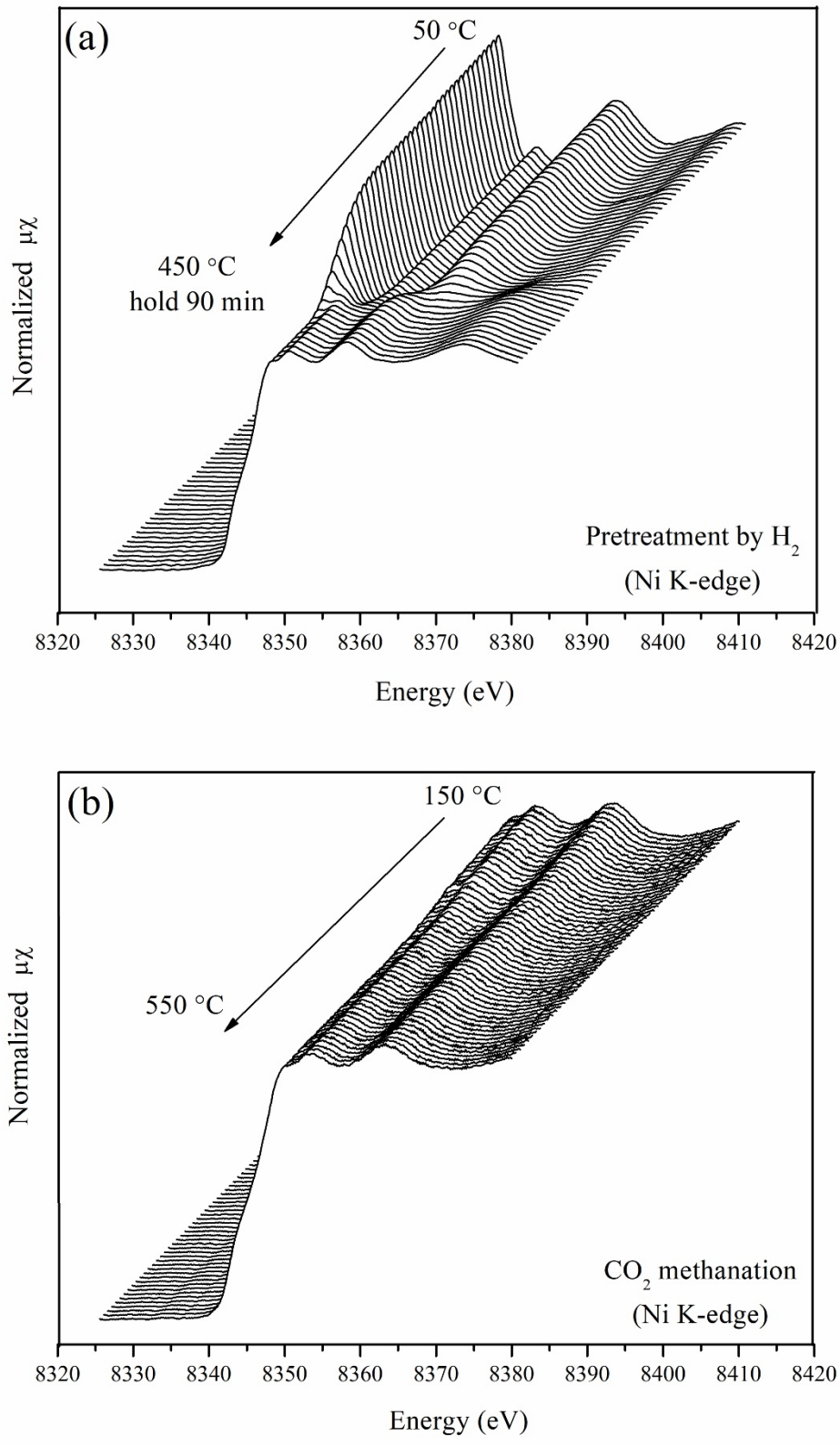

609 **Figure 15** in-situ Ni K-edge XANES spectra obtained from TR-XAS experiment of
610 20%wt Ni/TiO_2: (a) pretreatment condition and (b) CO_2 methanation.

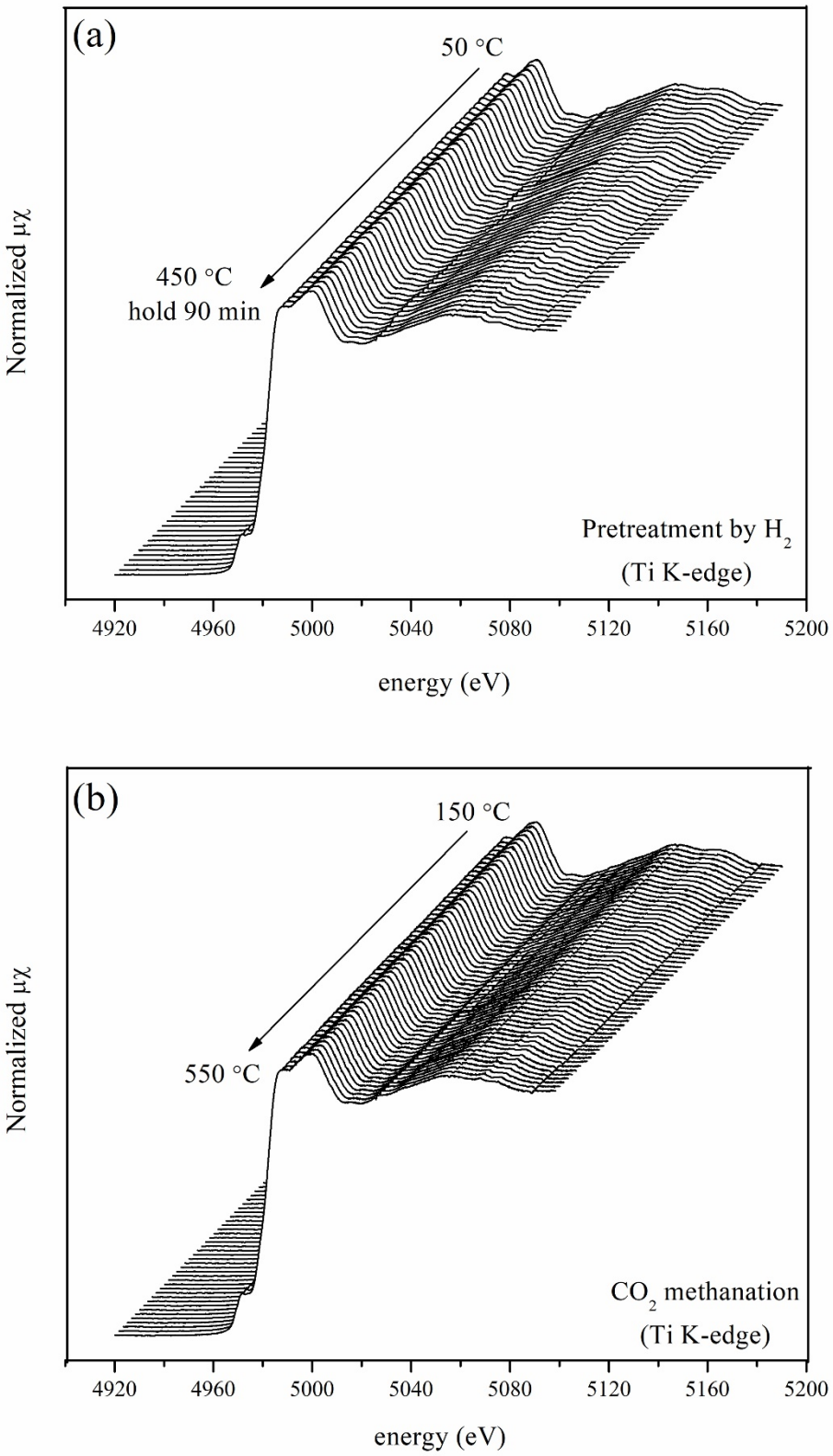

611 **Figure 16** in-situ Ti K-edge TR-XAS experiment of 20%wt Ni/TiO_2: (a) pretreatment
612 condition and (b) CO_2 methanation.
613

3.3.2 Extended X-ray absorption Fine Structure (EXAFS) study for monitoring Ni oxidation state during CO_2 methanation

Several works reported that Ni species on the catalyst surface is an important active site for enhancing CO_2 methanation rate since H_2 favors to adsorb on metal active site. Therefore, in this part, EXAFS analysis data was conducted to understand the state of Ni, structural changing of Ni during CO_2 methanation. The Fourier transformed function without phase correction of in-situ Ni K-edge EXAFS oscillation for 20wt% Ni/TiO_2 at the reaction temperature of 150, 350 and 550 °C is shown in Figure 17. The feature of all XANES spectra were similar to that of Ni foil. However, the amplitude of the spectra decreased with increased reaction temperature. Since, the amplitude is related to the coordination number around Ni probe atom, thus, EXAFS analysis can provide the information on the changing of Ni species during CO_2 methanation. The experimental data was normalized and the spectra were amplified by k^2 weight with R space window in the range of 1-5 Å and k range of 3-10 $Å^{-1}$. Figure 18(a) and 18(b) displays the k^2 weight and the radial function of Ni K-edge EXAFS spectra for 20wt% Ni/TiO_2, respectively. The calculated EXAFS of all catalysts were obtained by fitting with the cubic closed-packed (CCP) Ni structure. The best fitting analysis parameters are summarized in Table 4. The fitting results showed a first strongest peak at around 2.0 Å (2.48 Å from fitting) which assigned to a single scattering path of absorbing Ni atom with the nearest neighboring Ni atom (Ni–Ni). The calculated coordination number for Ni foil was 9.3 which indicated that Ni probe atom was surrounded by approximately 9 atoms. From Table 4, the calculated coordination number of 20wt% Ni/TiO_2 at 150, 350 and 550 °C were reduced to 7.6, 7.1 and 6.0, respectively. The lowering of coordination number of 20wt% Ni/TiO_2 with increasing of reaction temperature implied to higher level of unsaturated Ni–Ni coordination. High unsaturated of Ni–Ni coordination number can promote the dissociation of hydrogen on catalyst surface which can lead to high catalytic activity [45,46]. Therefore, high unsaturated Ni–Ni coordination number at high temperature (indicated by lowering of C.N.) provided high possibility of H_2 adsorption. However, the adsorption ability of H_2 on an active site was one of the factor to describe the catalytic performance. In order to describe the catalytic activities enhancement, understanding on the adsorption behavior of two reactants should be studied.

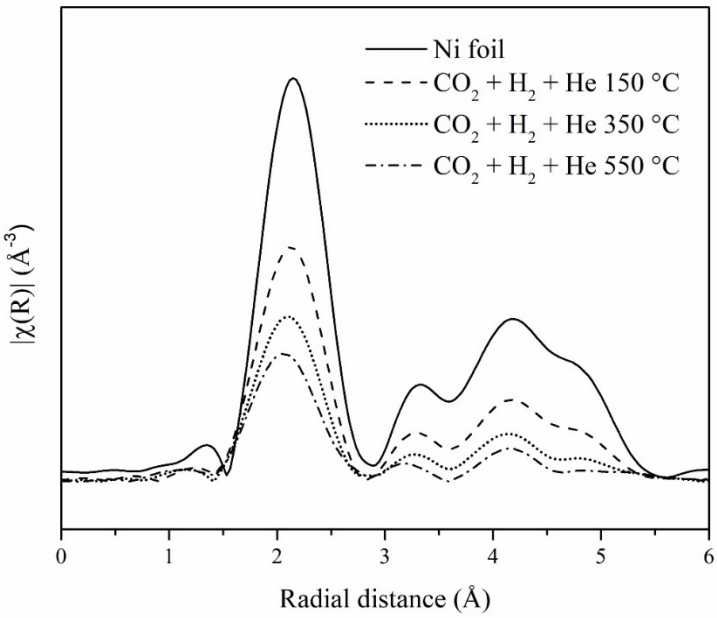

Figure 17 Fourier Transform functions of *in-situ* EXAFS oscillation (without phase collection) of Ni foil and 20wt% Ni/TiO_2 at 150, 350 and 550 °C under CO_2 methanation.

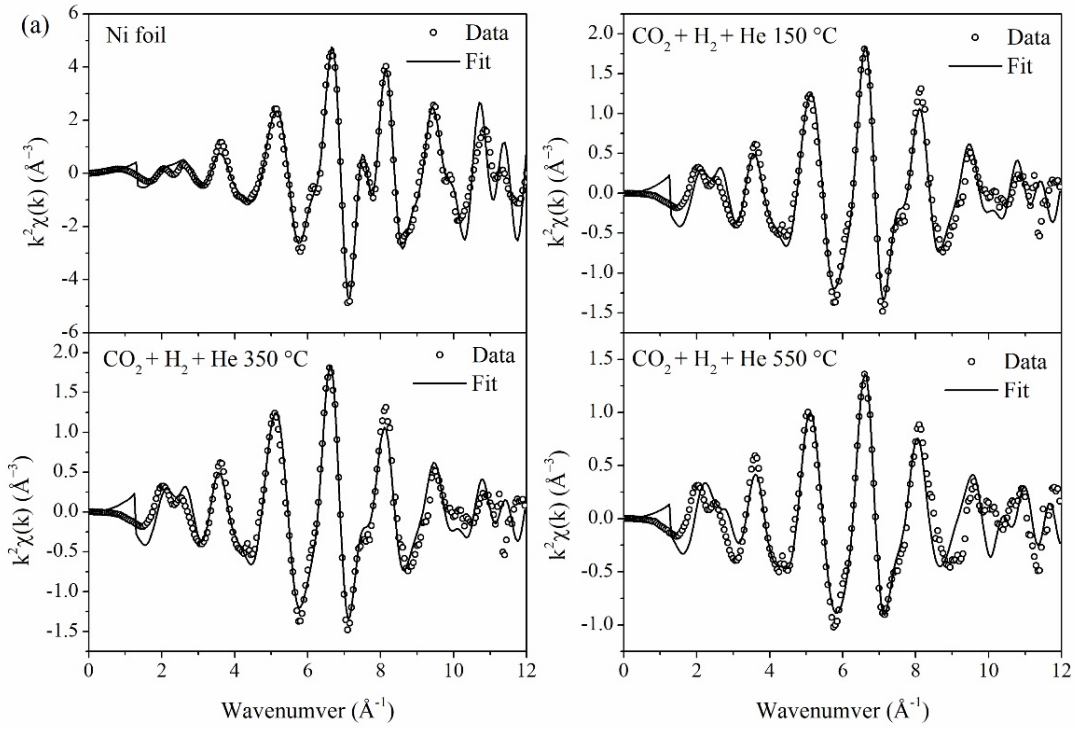

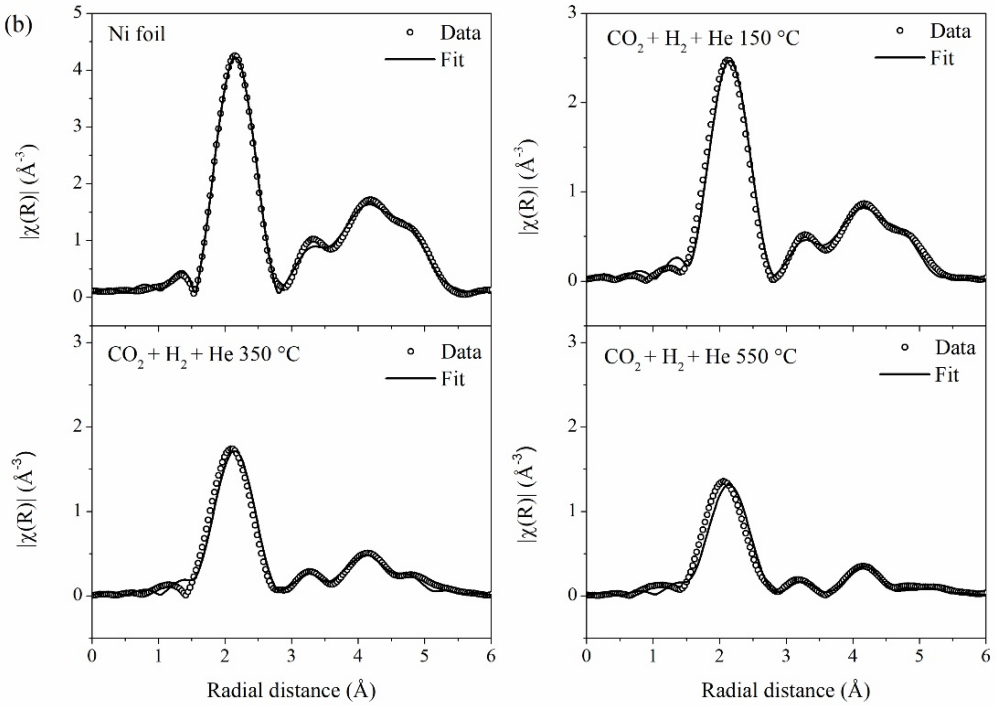

Figure 18 (a) The k^2 weight EXAFS spectra of 20wt% Ni/TiO_2 at 150, 350 and 550 °C under CO_2 methanation.

(b) The radial function of Ni K-edge EXAFS of 20wt% Ni/TiO_2 at 150, 350 and 550 °C under CO_2 methanation.

Table 4 The best fitting parameters of 20wt% Ni/TiO_2.

Samples	Shells	Best fit EXAFS parameters			
		N	σ^2	ΔE (eV)	R (Å)
Ni foil	Ni–Ni	9.3	0.0056	6.776	2.48
CO_2 + H_2 + He 150 °C	Ni–Ni	7.6	0.0088	6.417	2.48
CO_2 + H_2 + He 350 °C	Ni–Ni	7.1	0.0120	6.223	2.48
CO_2 + H_2 + He 550 °C	Ni–Ni	6.0	0.0130	6.240	2.48

3.4 The role of added Ni on enhancing CO_2 methanation

It has been reported that a different preparation method had a significant effect on physical and chemical properties of the catalysts which can be altered to the catalytic activities. In this work, sol-gel method was used to synthesize the catalyst for using in CO_2 methanation.

Since, this method is one of the reducible methods for preparing the catalyst, thus this method was employed. In the catalytic reaction, adsorption of the reactants on the catalyst surface is one of the most important elementary steps to control and dominate the catalytic reaction rate. Therefore, to speed up the reaction rate, enhancing the reactants adsorption ability on catalyst surface must be done. For CO_2 methanation, CO_2 and H_2 adsorption on catalyst surface can be enhanced by different approach. For CO_2 molecules, providing the basicity sites on the catalyst surface can increase the CO_2 adsorption capacity by acid-base interaction or existing of oxygen vacancy can also improve the adsorption capacity [47-49]. While H_2 molecules, it is known that H_2 favors to adsorb on metallic metal sites, especially on transition metals group, in dissociative form, thus dispersing of metal active sites on the catalyst surface can increase the H_2 adsorption capacity. Consequently, modification of the catalyst by above approaches would lead to increase of adsorption rate of reactants and also speed up the reaction rate. Preparation and modification by sol-gel method was used to alter the surface and catalyst properties which can provide both oxygen vacancies and metal active sites for CO_2 and H_2 adsorption, respectively. For CO_2 methanation, nickle was usually used to modify on support surface to increase the activity of the catalyst. In this work, added Ni on TiO_2 support acted as a bi-functional role in enhancing CO_2 methanation rate. First, addition of Ni during TiO_2 sol-gel process led to incorporation of Ni^{2+} into TiO_2 lattice and resulted in strain and unbalanced charge and then oxygen vacancy was formed (this result can be evidenced by EXAFS data.). The oxygen vacancy was an active site for CO_2 adsorption; i.e., CO_2 interacted with oxygen vacancies by strong interaction and weakened the C=O bond [50,51]. Second, the excess amount of added Ni was existed in NiO form which might be located on the catalyst surface and this NiO phase was an active site for H_2 adsorption (after reduction to Ni^0 by pretreatment process before starting the reaction). Moreover, increasing of NiO crystallinity upon increase of Ni content was observed (increase of NiO peak intensity in XRD pattern) which resulted in lowering or inhibiting of TiO_2 crystal growth [52]. From this effect, smaller crystalline size of TiO_2 was occurred and higher surface area was observed. Figure 19(a)-19(c) illustrates the comparison of CO_2 methanation catalytic activities between 20wt% Ni/TiO_2 obtained by sol-gel and impregnation method. It is seen that addition of Ni into TiO_2 support by sol-gel method exhibited higher catalytic activity than that by impregnation method. Although, impregnation method is one of the simplest preparation method but the obtained catalyst properties were lowered, especially surface area and porosity which was an important properties that can dominate to the reduction rate. From Figure 19(d)-19(e), beside the higher catalytic activity of

catalyst obtained from sol-gel method, this catalyst was more selectively toward to CH_4 than CO while the impregnated catalyst exhibited an opposite result.

In order to evidence the role of added Ni in enhancing the reaction rate, CO_2 and H_2 adsorption studies were conducted. Since, in catalyst cycle, the adsorption of reactants on catalyst surface is usually assigned as a rate determining step, therefore, investigation of adsorption process can provide the information that can be used to understand and describe the role of catalyst in enhancing the reaction rate. For CO_2 methanation, increasing of CO_2 and H_2 adsorption can enhance the reaction rate, since, higher amount of adsorbed CO_2 and H_2 on catalyst surface would lead to more possibility to react and convert to products. In the case of H_2 adsorption, the results are illustrated in H_2-chemisorption part and are summarized in Table 3. It is assumed that only H_2 was adsorbed on Ni active site, thus higher amount of H_2 chemisorbed would be implied to higher Ni active area on catalyst surface. The results from Table 3 showed that H_2 chemisorption amount was increased with increasing of Ni content (5.80, 13.8, 25.5 and 43.4 μmol g^{-1} for 3, 6, 12 and 20wt%, respectively). For CO_2 adsorption study, thermogravimetric analysis (TGA) was used. The CO_2 uptake experiment was conducted at 40 °C (the lowest temperature for the apparatus) and ambient pressure for 110 min. Figure 20 illustrates the data reduction from TGA experiment which expressed in the term of CO_2 uptake at interval time. The results showed that the CO_2 uptake increased with time and almost constant within 60 min. The amount of CO_2 uptake was increased with Ni content (0.189, 0248, 0.349 and 0.377 mmol g^{-1} for 0, 3, 6 and 12wt% Ni, respectively). The results from XRD and EXAFS indicated that added Ni^{2+} was substituted into TiO_2 lattice and led to formation of oxygen vacancies which was reactive for CO_2 adsorption. However, increased Ni content up to 20wt%, the CO_2 uptake was slightly dropped. This result can be used to relate with the highest catalytic activities of 20wt% Ni/TiO_2. Since, the adsorption sites for CO_2 and H_2 were co-exist on the catalyst surface then if higher amount of adsorbed CO_2, inhibition and suppression of H_2 adsorption on metal active site was probably occurred and then led to decrease of surface reaction between adsorbed CO_2 and H_2 and finally lower the catalytic activity. Therefore, an appropriate amount of adsorbed CO_2 and H_2 on catalyst surface would lead to high catalytic activities. Figure 21 shows the relationship between H_2 chemisorption and CO_2 uptake as a function of Ni content. It was found that 20wt% Ni/TiO_2 can maximize the CO_2 methanation rate. This result caused from the improvement of catalyst properties by addition of Ni which led to existence of active sites with appropriate performance to promote the CO_2 and H_2 adsorption.

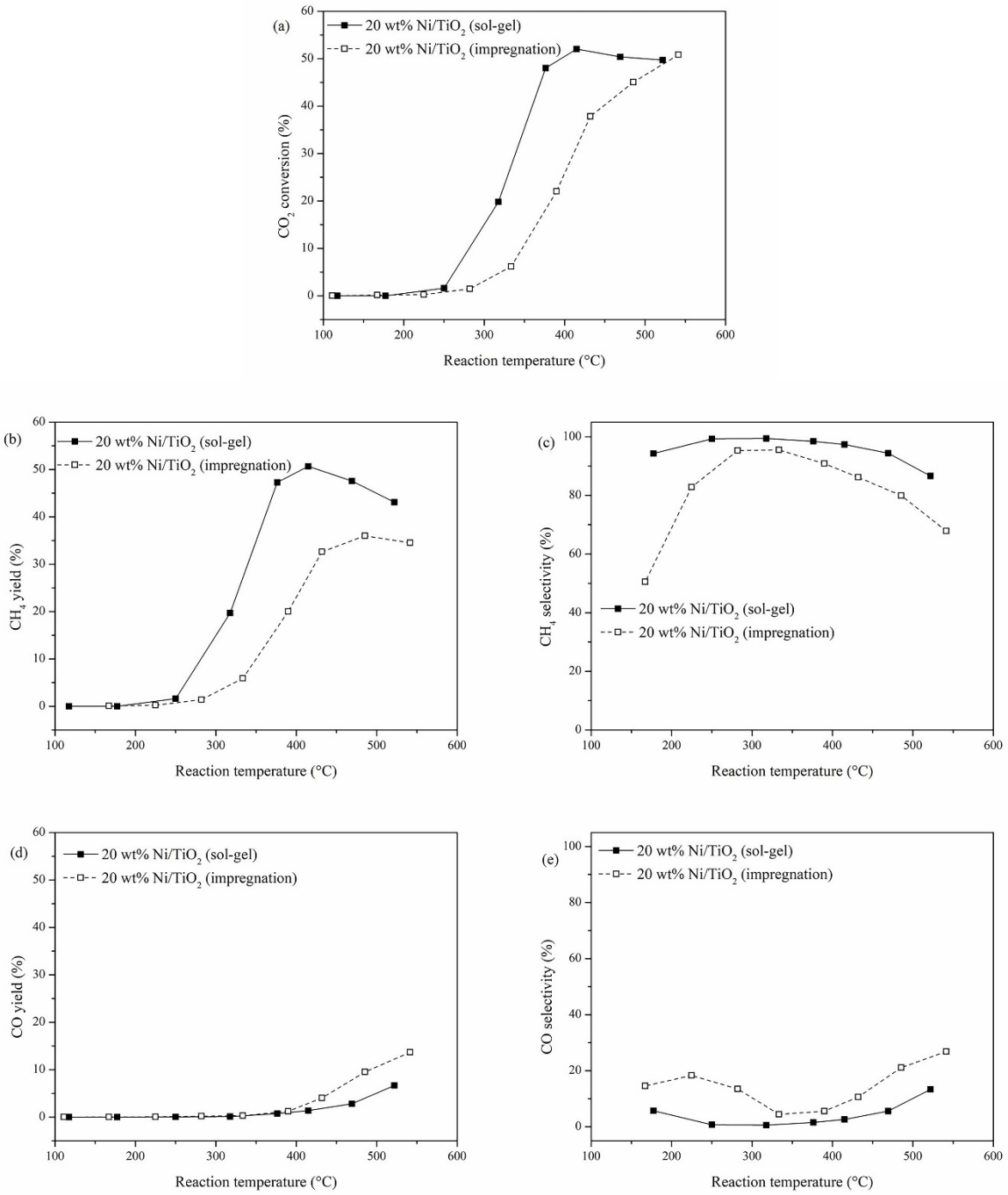

Figure 19 (a) CO_2 conversion, (b) CH_4 yield, (c) CH_4 selectivity, (d) CO yield and (e) CO selectivity of 20wt% Ni-loaded TiO_2 by preparing with different preparation methods; sol-gel and impregnation. The H_2/CO_2/He ratio was 24:6:10, total flow rate was 40 mL min^{-1} and WHSV was 48,000 mL g^{-1} h^{-1} at reaction temperature 100-550 °C.

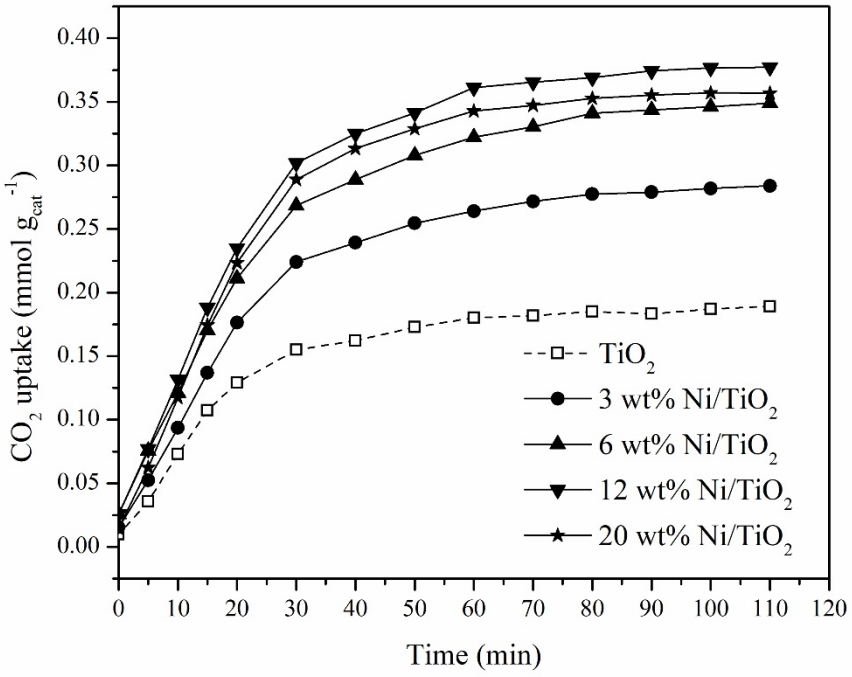

730 **Figure 20** CO_2 uptake from TGA experiment for 0, 3, 6, 12 and 20wt% Ni/TiO_2.

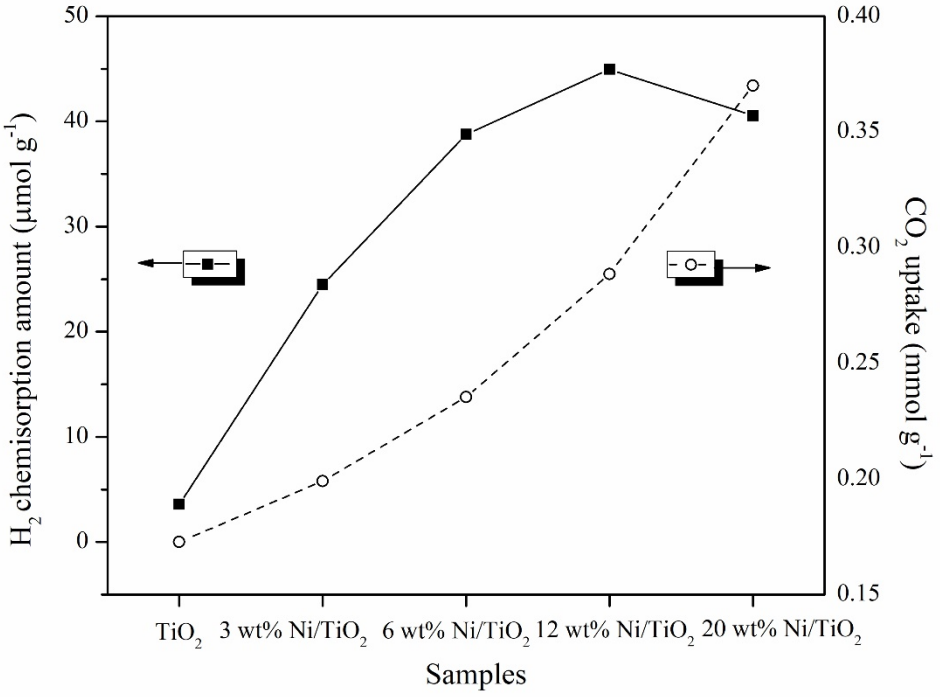

731 **Figure 21** The relationship between H_2 chemisorption and CO_2 uptake as a function of Ni
732 content.

733

4. Conclusion

In this work, the role of added Ni into TiO_2 support in enhancing CO_2 methanation rate was studied. The Ni supported TiO_2 with different amount of Ni loading as 3, 6, 12 and 20wt% Ni were synthesized by sol-gel method. The preparation method by addition of Ni during TiO_2 sol-gel process led to structural and surface properties changing which could alter to their catalytic activities. The results show that added Ni modified the catalyst properties in 2 ways; i) Ni^{2+} was substituted into TiO_2 lattice which led to strain and unbalanced charge and then creating the oxygen vacancy. This effect can be evidenced by the results from distortion of Ti–O, Ti–Ti bond length (EXAFS analysis) and the enlargement of TiO_2 unit cell (XRD results). ii) upon increasing of Ni content, the excess amount of Ni was presented in NiO formed and probably located on the catalyst surface. This can be seen from the diffraction peak of NiO in XRD pattern. Moreover, the crystallinity of NiO increased with increasing Ni content which could inhibit to TiO_2 crystal growth and resulted in smaller TiO_2 crystalline sizes and then higher surface area was occurred. The existence of oxygen vacancy and NiO phase can be evidenced by XANES linear combination analysis. The results showed that NiO phase was increased with increasing of Ni loading. These two species that produced from addition of Ni during TiO_2 sol-gel process has a significant role in enhancing the CO_2 methanation rate. Both oxygen vacancy and NiO phase were an active site for promoting the adsorption of CO_2 and H_2 on catalyst surface, high possibility of surface reaction between these two adsorbed species were occurred and finally the reaction rate was enhanced. However, excess amount of adsorbed CO_2 on surface can inhibit the H_2 adsorption and lead to lowering of CO_2 rate.

Acknowledgements

The authors gratefully acknowledge the facility support from Khon Kaen University, Institute for catalysis (Hokkaido University, Japan) for X-ray diffraction and N_2 adsorption-desorption analysis and Synchrotron Light Research Institute (Public Organization), Nakhon Ratchasima, Thailand for XAS analysis.

Reference

[1] J. Gao, Y. Wang, Y. Ping, D. Hu, G. Xu, F. Gu, F. Su, RSC Adv. 2, (2012), 2358-2368.

[2] W. Li, H. Wang, X. Jiang, J. Zhu, Z. Liu, X. Gao, C. Song, RSC Adv. 8, (2018), 7651-7669.

[3] J. Gao, Q. Liu, F. Gu, B. Liu, Z. Zhong, F. Su, RSC Adv. 5, (2015), 22759-22776.

[4] M.S. Duyar, A. Ramachandran, C. Wang, R.J. Farrauto, J. CO_2 Util. 12, (2015), 27-33.

[5] D.C. Upham, A.R. Derk, S. Sharma, H. Metiu, E.W. McFarland, Catal. Sci. Technol. 5, (2015), 1783-1791.

[6] M. Schubert, S. Pokhrel, A. Thomé, V. Zielasek, T.M. Gesing, F. Roessner, L. Mädler, M. Bäumer, Cat. Sci. Technol. 6, (2016), 7449-7460.

[7] P. Panagiotopoulou, Appl., Catal. A. 542, (2017), 63-70.

[8] J. Gao, Q. Liu, F. Gu, B. Liu, Z. Zhong, F. Su, RSC Adv. 5, (2015), 22759-22776.

[9] H.C. Wu, Y.C. Chang, J.H. Wu, J.H. Lin, I.K. Lin, C.S. Chen, Catal. Sci. Technol. 5, (2015), 4154-4163.

[10] R. Zhou, N. Rui, Z. Fan, C.J. Liu, Int. J. Hydrogen Energy. 41, (2016), 22017-22025.

[11] J. Ashok, M.L. Ang, S. Kawi, Catal. Today. 281, (2017), 304-311.

[12] L.A.A. Varilla, N. Seriani, J.A. Montoya, J. Mol. Model. 25, (2019), 1-8.

[13] Y.X. Pan, C.J. Kia, D. Mei, Q. Ge, Langmuir. 26, (2010), 5551-5558.

[14] X. Li, Z.J. Zhao, L. Zeng, J. Zhao, H. Tian, S. Chen, K. Li, S. Sang, J. Gong. Chem. Sci., 9, (2018), 3426-3437.

[15] B. Li, H. Metiu, J. Phys. Chem. 114, (2010), 12234-12244.

[16] X. Yan, Y. Liu, B. Zhao, Z. Wang, Y. Wang, C.J. Lia, Int. J. Hydrogen Energy. 38, (2013), 2283-2291.

[17] A. Niltrarach, S. Kityakarn, A. Worayingyong, J.T. Thienprasert, W. Klysubun, P. Songsiriritthigul, S. Limpijumnong. Phys B Condens Matter. 407, (2012), 2915-2918.

[18] X. Su, J. Xu, B. Liang, H. Duan, B. Hou, J. Energy. Chem. 25, (2016), 553-565.

[19] Q. Liu, J. Gao, F. Gu, X. Lu, Y. Liu, H. Li, Z. Zhong, B. Liu, G. Xu, F. Su, J. Catal. 326, (2015), 127-138.

[20] P. Kidkhunthod, Adv. Nat. Sci. Nanosci. Nanotechnol. 8 (2017).

[21] W. Klysubun, P. Kidkhunthod, P. Tarawarakarn, P. Sombunchoo, C. Kongmark, S. Limpijumnong, S. Rujirawat, R. Yimnirun, G. Tumcharern, K. Faungnawakij, J. Synchrotron Radiat. 24, (2017), 707-716.

[22] X. Gao, A. Traitangwong, M. Hu, C. Zuo, V. Meeyoo, Z. Peng, C. Li, Energy Fuels. 32, (2018), 3681-3689.

[23] V.R. Akshay, B. Arun, G. Mandal, M. Vasandhara, Phys. Chem. Chem. Phys. 21, (2019), 2519-2532.

[24] M. Manzoor, A. Rafiq, M. Ikram, M. Nafees, S. Ali, Int. Nano Lett, 8, (2018), 1-8.

[25] I. Ganesh, A.K. Kumar, P.P. Kumar, P.S.C. Sekhar, K. Radha, G. Padmanabham, G. Sundararajan, Sci World J. 2012, 2012, 13-20.

[26] P.M. Shirage, A.K. Rana, Y. Kumar, S. Sen, S.G. Leonardi, G. Neri, RCS Adv. 6, (2016), 82733-82742.

[27] K.C. Chanapattharapol, S. Krachuamram, Y. Poo-arporn, Solid State Sci. 99, (2020), 106066.

[28] S. Tiwari, G. Bajpai, T. Srivastava, S. Viswakarma, P. Shirage, S. Sen, S. Biring, Scr. Mater. 129, (2017), 84-87.

[29] S.V. Moghaddam, M. Rezaei, F. Meshkani, R. Daroughegi, Int. J. Hydrogen Energy. 43, (2018), 16522-16533.

[30] J. van de Loosdrecht, A.M. van de Kraan, A.J. van Dillen, J.W. Geus, J. Catal. 170, (1997), 217-226.

[31] S.W. Ho, C.Y. Chu, S.G. Chen, J. Catal. 178, (1998), 34-48.

[32] J. Liu, C. Li, F. Weng, S. He, H. Chen, Y. Zhao, M. Wei, D.G. Evans, X. Duan, Catal. Sci. Technol. 3, (2013), 2627-2633.

[33] X. Meng, C. Wan, Y. Wang, X. Ju, J. Alloys Comp. 735, (2018), 1637-1647.

[34] K.I. Pandya, R.W. Hoffman, J. McBeen, W.E. O'Grady, J. Electrochem. Soc. 137, 1990, 383-388.

[35] F. Farges, G.E. Brown Jr, J.J. Rehr, Phys. Rev. B. 56, (1997), 1809-1819.

[36] A. Sharma, M. Varshney, H.J. Shin, B.H. Lee, K.H. Chae, S. O. Won, Mater. Chem. Phys.191, (2017), 129-144.

[37] J.H. Yang, H. Piao, A. Vinu, A.A. Elzatahty, S.M. Paek, J.H. Choy, RCS, Adv. 5, (2015), 8210-8215.

[38] B. Bharti, S. Kumar, H.N. Lee, R. Kumar, Sci Rep, 6, (2016), 1-12.

[39] M. Sahoo, A.K. Yadav, S. Ghosh, S.N. Jha, D. Bhattacharyya, T. Mathews, Phys. Chem. Chem. Chem. Phys. 21, (2019), 6198-6206.

[40] B.J. Hsieh, M.C. Tsai, C.J. Pan, W.N. Su, J. Rick, J.F. Lee, Y.W. Yang, B.J. Hwang, NPG Asia Mat, 9, (2017), e403.

[41] K. Huang, K. Sasaki, R.R. Adzic, Y. Xing, J. Mater. Chem. 22, (2012), 16824-16832.

[42] H. Song, T.G. Jeong, Y.H. Moon, H.W. Chun, K.Y. Chung, H.S. Kim, B.W. Cho, Y.T. Kim, Sci. Rep. 4, (2015), 1-8.

[43] L. Huang, L. Yan, M. Tang, G. Wang, Z. Qin, H. Ge, ACS Omega, 3, (2018), 18967-18975)

[44] J.A. Rodriguez, J.C. Hanson, A.I. Frenkel, J.Y. Kim, M. Pe´rez, J. Am. Chem. Soc, 124, (2002), 346-354.

[45] D. Hu, J. Gao, Y. Ping, L. Jia, P. Gunawan, Z. Zhong, G. Xu, F. Gu, F. Su, Ind. Eng. Chem. Res. 51, (2012), 4875-4886.

[46] P. van Helden, J.A. van den Berg, I.M. Ciobıˆcaˇ, Catal. Sci. Technol. 2, (2012) 491-494.

[47] W. Göpel, G. Rocker, R. Feierabend, Phys. Rev. B. 28, (1983), 3427-3438.

[48] J. Xu, X. Su, H. Duan, B. Hou, Q. Lin, X. Liu, X. Pan, G. Pei, H. Geng, Y. Huang, T. Zhang, J. Catal. 333, (2016), 227-237.

[49] X. Jia, X. Zhang, N. Rui, X. Hu, C. Liu, Appl. Catal. B Environ. 244, (2019), 159-169.

[50] F. Wang, S. He, H. Chen, B. Wang, L. Zheng, M. Wei, D.G. Evans, X. Duan, J. Am. Chem. Soc. 138, (2016), 6298-6305.

[51] M.Y.S. Hamid, M.L. Firmansyah, S. Triwahyono, A.A. Jalil, R.R. Mukti, E. Febriyanti, V. Suendo, H.D. Setiabudi, M. Mohamed, W. Nabgan, Appl. Catal. A. 532, (2017), 86-94.

[52] M. Pudukudy, Z. Yaakob, A. Kadier, M.S. Takriff, N.S.M. Hassan, Int. J. Hydrogen Energy. 42, (2017), 16495-16513.